

Thermal properties of asymmetric nuclear matter

A. Fedoseew¹ and H. Lenske^{1,2}¹*Institut für Theoretische Physik, Universität Gießen Heinrich-Buff-Ring 16, D-35392 Gießen, Germany*²*GSI Helmholtzzentrum für Schwerionenforschung, Planckstraße 1, 64291 Darmstadt, Germany*

(Received 13 August 2014; revised manuscript received 10 February 2015; published 3 March 2015)

The thermal properties of asymmetric nuclear matter are investigated in a relativistic mean-field approach. We start from free-space NN interactions and derive in-medium self-energies by the Dirac-Brueckner theory. By the density-dependent relativistic hadron procedure we derive in a self-consistent approach density-dependent meson-baryon vertices. At the mean-field level, we include isoscalar and isovector-scalar and vector interactions. The nuclear equation of state is investigated for a large range of total baryon densities up to the neutron star regime, the full range of asymmetries $\xi = Z/A$ from symmetric nuclear matter to pure neutron matter, and temperatures up to $T \sim 100$ MeV. The isovector-scalar self-energies are found to modify strongly the thermal properties of asymmetric nuclear matter. A striking result is the change of phase transitions when isovector-scalar self-energies are included.

DOI: [10.1103/PhysRevC.91.034307](https://doi.org/10.1103/PhysRevC.91.034307)

PACS number(s): 21.65.-f, 21.30.Fe, 21.60.-n

I. INTRODUCTION

A major task of nuclear many-body theory is to understand the equilibrium properties of nuclear matter under variations of density, pressure, proton-to-neutron fraction, and, last but not least, temperature. For this demanding goal, decadelong experimental and theoretical efforts have been made, ranging from early studies of compound nuclei and highly excited precompound systems to studies of exotic nuclei at extreme isospin and compressed baryonic matter in high-energy heavy-ion collisions. Considering the status of research on the nuclear equation of state (EOS) one finds that many theoretical studies exist for symmetric and pure neutron matter. The work of Sauer *et al.* [1] is probably the first systematic study to derive the thermal properties of finite nuclei on theoretical grounds. Actually, historically, nuclear-matter studies were strongly motivated by astrophysical issues [2], with a special need for investigations of asymmetric matter with arbitrary values of the charge asymmetry defined in terms of the proton fraction $\xi = \frac{Z}{A}$, ranging from $\xi = \frac{1}{2}$ in symmetric matter to $\xi = 0$ for pure neutron matter. Thermodynamically, symmetric nuclear matter and pure neutron matter, respectively, correspond to single-fluid systems. Because in symmetric nuclear-matter isovector self-energies are absent by symmetry reasons, protons and neutrons are dynamically indistinguishable and hence form a single-component fluid. The one-component character of neutron matter is obvious. The theoretical description of such one-component quantum systems is much simpler than that of a multicomponent fluid. As is well known and is seen also in later sections of this work, first, the treatment of asymmetric nuclear matter requires extended theoretical methods and, second, such a two-fluid system shows new features which are absent (or hidden by symmetry reasons) in single-fluid nuclear matter.

Equilibrium thermodynamics, as pursued here, is the appropriate approach to the nuclear EOS as a function of density and temperature. Known essential properties are the liquid-gas phase transition at subsaturation densities and moderate temperatures. An important question is how the system evolves by passing various *binodals*, denoting phase-separation bound-

aries, and *spinodals*, indicating stability or, likewise, instability boundaries. Studies of infinite and finite nuclear systems indicate that symmetric nuclear matter undergoes a liquid-gas phase transition at critical temperatures in the range of $T_C = 10\text{--}20$ MeV [2,3]. The results depend, however, on the chosen NN interaction. Phenomenological density functional models seem to favor lower $T_C \sim 10$ MeV, as in the very early work of Sauer *et al.* [1], while values around $T_C \sim 20$ MeV are predicted by microscopic approaches as, for example, in the study of Baldo and Ferreira [3]. Covariant field theory and thermodynamics have been studied very frequently. A comprehensive discussion is found in the early work of Weldon [4]. The connection of a hadron-field theory and thermodynamics was discussed by Furnstahl and Serot [5]. Finite-temperature many-body theory, the Green's functions, and the solution of the G -matrix equation in a transport theoretical connection has been reviewed in detail by Botermans and Malfliet [6]. The same authors have studied intensively in-medium interactions in cold and hot nuclear matter [7,8]. As reported in Ref. [8], they found that the Dirac-Brueckner G matrix depends only very weakly on temperature. As discussed later, this makes it possible to extrapolate interactions safely from the $T = 0$ to the $T > 0$ case. The work of Müller and Serot [9] addresses the thermal properties of asymmetric nuclear matter quite generally. On the basis of a relativistic mean-field model with nonlinear self-interactions of the scalar and vector fields and relativistic thermodynamics, the phase structure of nuclear matter with arbitrary proton content was investigated in detail. An unexpected result was that in asymmetric matter instabilities are induced primarily by fluctuations in the proton content rather than by fluctuations in the net baryon density. Hence, *chemical instability* of the composition of the fluid wins over the *mechanical instability* of the total system, at least in that particular model. The instability region of warm asymmetric nuclear matter has been studied by many other groups. A detailed comparison between relativistic models and Skyrme forces is provided by the work of Dutra *et al.* [10].

The mentioned properties are largely determined by the NN interactions, besides, naturally, Fermi-Dirac statistics. At the

energy and momentum scales relevant for nuclear matter, NN forces are acting like van der Waals forces among molecules. Hence, at not-too-high density, pressure, and temperature nuclear matter resembles a multicomponent van der Waals gas. However, the exact values of the permissible density and temperature ranges are yet to be determined. It is one purpose of this work to add new aspects to that ongoing research program. As far as temperature is concerned, the QCD phase transition into a quark-gluon plasma (QGP) at $T_c^{\text{QCD}} \sim 150$ MeV is a clear limit. Hence, only temperatures well below T_c^{QCD} should be considered. We choose a temperature range $T < 100$ MeV. The density behavior is much less constraint. The assumed central density of a neutron star may serve as guideline. Taking into account the recently observed neutron star with a mass of twice the solar mass, we may accept a density range below $6\rho_{eq}$, where $\rho_{eq} = 0.16 \text{ fm}^{-3}$ is the density of symmetric nuclear-matter density at the saturation point.

In addition to the liquid-gas phase transition, equilibrated nuclear matter may undergo other phase transitions by creating hadrons. Pion and kaon condensation has been investigated theoretically, and also the thermal production of excited baryons like the $\Delta(1232)$ resonance was considered. However, clear experimental signals indicating such hadron condensation with the sudden appearance of a new type of species in the fluid are still missing. Better established are bosonization processes in cold matter at extremely low densities: Under such conditions nuclear matter rearranges into bound constituents, forming deuterons and, especially, α particles. In the crust of neutron stars, one expects a lattice of heavier nuclei up to the iron and nickel region [11]. Finite temperature effects on the geometrical formation of the neutron star crust have been analyzed in detail by Gögelein *et al.* [12]. Here we consider pure uniform nuclear matter, composed of nucleonic quasiparticles only but with an arbitrary mixture of protons and neutrons. A very complete and comprehensive discussion of thermal dynamics in asymmetric nuclear matter is found in the already cited work by Müller and Serot [9]. These authors have pointed out in remarkable clarity the important differences between the thermodynamics of symmetric and pure neutron matter on the one side and the thermodynamics of asymmetric matter. Symmetric and neutron matter as single-component systems with a single conserved charge, namely baryon number, correspond to a pure classical van der Waals gas. As the latter, symmetric and neutron matter develop first-order phase transitions. This is no longer the case for multicomponent systems as asymmetric nuclear matter, where protons and neutrons occupy in momentum space different Fermi spheres. Within the relativistic mean-field model used in Ref. [9], quantal multicomponent systems change their state of aggregation by second-order phase transitions. Hence, if a phase transition is going to happen in a charge-asymmetric nuclear system, signals will be washed out, complicating the identification of critical phenomena. Clearly, this is a strict result only for equilibrium thermodynamics based on consideration of infinite matter. Transportlike nonequilibrium conditions as encountered in a heavy-ion collision underlie their own special dynamical and statistical laws as, e.g., in fragmentation reactions [13–15]. Interestingly, as discussed in

those papers, grand-canonical thermodynamics is a successful concept also for fragmentation processes.

The investigations in Ref. [9] are based on the nonlinear extension of the original Walecka model, allowing for self-interactions of the scalar-isoscalar field. Those approaches are completely phenomenological in nature without attempting to relate the model parameters to an underlying theory. Here we follow a different approach by using the density-dependent relativistic hadron (DDRH) nuclear-field theory providing an easy-to-handle and flexible description of equilibrated cold and hot nuclear matter. DDRH theory, developed some time ago in Giessen [16–20], is a density-dependent field theory with interactions derived by Dirac-Brueckner theory from free-space NN interactions. The one-boson exchange picture on which DDRH theory is based, gives access to the full spectrum of scalar, pseudoscalar, and vector interaction channels, typically described in terms of meson-exchange interactions. The medium dependence is taken into account by vertex functionals depending on Lorentz-invariant binomials of the baryon-field operators. Their mean-field expectation values are evaluated by relations using the self-consistent scheme of Dirac-Brueckner Hartree-Fock (DBHF) theory. In this sense, the DDRH field theory is a parameter-free *ab initio* description of nuclear matter. In particular, the microscopic ansatz gives access to details unreachable for phenomenological approaches. One of those regions is the contribution of isovector-scalar interactions as realized in nature by the $a_0(980)$ meson. The importance of the corresponding scalar-isovector mean field for asymmetric nuclear matter was pointed out in our previous work [19,20], deriving for the first time the density dependence of the δ - NN vertex by DBHF calculations. Since then, the interaction channel is being included as a standard tool in many nuclear interaction studies, see, e.g., Refs. [21,22]. Obviously, this is a short-range phenomenon acting in competition with the vector meson repulsion. However, the consequences are quite different and important: Scalar fields modify the relativistic effective masses of baryons. Hence, they change the mechanical properties. Because isovector-scalar fields lead in asymmetric nuclear matter to counterbalanced modifications of proton and neutron effective masses, we have to expect important modifications of the dynamical and, especially, the thermodynamical laws. Here we present for the first time extensions of DDRH theory to equilibrated nuclear matter at finite temperature. To a large extent, the results obtained in the present work are representative for any type of nuclear-field theory based on density-dependent meson-baryon vertices. However, an essential and unique feature over other work is the inclusion of scalar-isovector interactions. In a relativistic approach the corresponding self-energies are leading to a splitting of the proton and neutron relativistic effective masses in asymmetric matter, thus changing the inertial properties of the particle species in an asymmetric manner. An important built-in property of DDRH theory is the conservation of the Hugenholtz-van Hove (HVH) theorem [23]. Rearrangement self-energies, accounting for the static polarization of the medium, are playing the essential role [17] in conserving the HVH relation. Because thermodynamical consistency is fulfilled at all densities and temperatures, we are avoiding

artificial effects from violations of the HVH theorem which will appear inevitably when density-dependent effective interactions like a Brueckner G matrix are used but rearrangement self-energies are neglected.

The nuclear many-body theoretical background is discussed in Sec. II; the relevant thermodynamical quantities are introduced in Sec. III. In Sec. IV we present our results on the EOS in mean-field approximation of symmetric nuclear matter and in Sec. V those for asymmetric nuclear matter. We also compare the DDRH results to those obtained from the DD-ME2 model [24], which is a phenomenological derivative of our DDRH theory. In this model the density-dependent vertices are fitted directly to nuclear data. Typically, DD-ME models neglect the δ mean field. Additionally, to emphasize the impact of the density-dependent formulation on various properties of nuclear matter, the results from the NL3 [25], the QHD model with constant interaction vertices [26], and the nonrelativistic Skyrme type model [27] are shown. For this purpose, we use the QHD model with σ , ω , and ρ mesons in its original formulation [26,28]. In particular, we discuss the influence of the isovector-scalar self-energies on the binodal and spinodal structures. Conclusions are drawn and an outlook is given to open questions and future work in Sec. VI.

II. DENSITY-DEPENDENT HADRON-FIELD THEORY

A. The DDRH Lagrangian and energy momentum tensor

An important step forward in understanding the saturation properties of infinite nuclear matter was achieved by theories describing in-medium interactions microscopically. Using relativistic Dirac-Brueckner (DB) it was found that the pertinent problem of nonrelativistic G -matrix calculations, namely, by always ending up at the Coester line and missing the empirical saturation point of infinite nuclear matter, could be overcome. With standard free-space NN interactions, reproducing well the NN scattering observables, the empirical saturation properties of nuclear matter could be described convincingly well [19,29–34]. Using realistic nucleon-nucleon meson-exchange potentials, in-medium interactions are derived by complete resummation of (two-body) ladder diagrams. Because full-scale DB calculations for finite heavy nuclei are not feasible, a practical approach is to derive from infinite-matter DB results an equivalent energy density functional. The Kohn-Sham [35] and the Hohenberg-Kohn [36] theorems confirm the existence of a general density functional, although they do not provide a guideline for construction. Based on the work in Refs. [33,37], we have derived in Refs. [16,17] a fully covariant and thermodynamically consistent field theory by treating the interaction vertices as Lorentz-scalar functionals of the nucleonic field operators. The DDRH approach, unlike common relativistic mean-field (RMF) models, accounts for quantal fluctuations of the baryon fields even in the ground state. In Ref. [18] the DDRH theory has been applied to asymmetric nuclear matter and nuclei far from stability. An appropriate set of coupling constants has been derived, now including isoscalar (σ , ω) and isovector (δ , ρ) vertices. In turn, a phenomenological approach to DDRH theory was proposed by Typel and Wolter [38], trying to derive the density

dependence of the vertices empirically by fits to nuclear data. Since then, a large variety of purely phenomenological models has been formulated by several groups and is being applied successfully to nuclei over almost the full mass table.

In the fully microscopic *ab initio* approach of the DDRH theory, one considers nuclear systems composed of protons and neutrons, described by Dirac field operators Ψ_q with $q = p, n$. Interactions are derived in the one-boson exchange approximation by using a set of mesons, mainly acting as virtual fields and thus providing the interactions among the nucleons. Our relativistic boson exchange model includes pseudoscalar (π, η), scalar [$\sigma, \delta/a_0(980)$], and vector mesons (ω, ρ). The Lagrangian is given by

$$\mathcal{L} = \mathcal{L}_N + \mathcal{L}_M + \mathcal{L}_{\text{int}}. \quad (2.1)$$

The fermionic part for the matter fields Ψ_q is of standard Dirac form:

$$\mathcal{L}_N = \sum_{q=p,n} \bar{\Psi}_q (i\gamma_\mu \partial^\mu - M_q) \Psi_q. \quad (2.2)$$

In the meson sector of the theory we have to distinguish the scalar [$\alpha = \sigma, \delta/a_0(980)$] and pseudoscalar ($\alpha = \eta, \pi$) mesons, obeying equations of the type

$$\mathcal{L}_M^{(\alpha)} = \frac{1}{2} (\partial_\mu \varphi_\alpha \partial^\mu \varphi_\alpha - m_\alpha^2 \varphi_\alpha^2). \quad (2.3)$$

The vector mesons ($v = \omega, \rho$) are subject to

$$\mathcal{L}_M^{(v)} = -\frac{1}{2} (F_{\mu\nu}^{(v)} F^{(v)\mu\nu} - m_v^2 A_\mu^{(v)} A^{(v)\mu}), \quad (2.4)$$

with the field strength tensors of the vector mesons,

$$\begin{aligned} F_{\mu\nu}^{(\omega)} &= \partial_\mu A_\nu^{(\omega)} - \partial_\nu A_\mu^{(\omega)}, \\ F_{\mu\nu}^{(\rho)} &= \partial_\mu A_\nu^{(\rho)} - \partial_\nu A_\mu^{(\rho)} - \hat{\Gamma}_\rho(\hat{\rho})(A_\mu^{(\rho)} \times A_\nu^{(\rho)}), \end{aligned} \quad (2.5)$$

where the ρ -meson field tensor includes the non-Abelian isospin term assuming the coupling to the conserved isovector current. Note, however, that the self-interaction term does not contribute in mean-field approximation.

Of special interest is the interaction part $\mathcal{L}_{\text{int}} = \mathcal{L}_{ps} + \mathcal{L}_s + \mathcal{L}_v$, which includes the pseudoscalar vertices,

$$\begin{aligned} \mathcal{L}_{ps} &= \hat{\Gamma}_\eta(\hat{\rho}) \bar{\Psi} \gamma_5 \Psi \varphi_\eta + \frac{f_\eta}{m_\eta} \bar{\Psi} \gamma_5 \gamma_\mu \Psi \partial^\mu \varphi_{ps} \\ &+ \hat{\Gamma}_\pi(\hat{\rho}) \bar{\Psi} \gamma_5 \boldsymbol{\tau} \Psi \boldsymbol{\varphi}_\pi + \frac{f_\pi}{m_\pi} \bar{\Psi} \gamma_5 \gamma_\mu \boldsymbol{\tau} \Psi \partial^\mu \boldsymbol{\varphi}_\pi, \end{aligned} \quad (2.6)$$

the scalar vertices,

$$\mathcal{L}_s = \hat{\Gamma}_s(\hat{\rho}) \bar{\Psi} \Psi \varphi_s + \hat{\Gamma}_\delta(\hat{\rho}) \bar{\Psi} \boldsymbol{\tau} \Psi \boldsymbol{\varphi}_\delta, \quad (2.7)$$

and the vector meson interactions, respectively,

$$\begin{aligned} \mathcal{L}_v &= \hat{\Gamma}_\omega(\hat{\rho}) \left(\bar{\Psi} \gamma_\mu \Psi A^{(\omega)\mu} + \frac{f_\omega}{m_\omega} \bar{\Psi} \sigma_{\mu\nu} \Psi F^{(\omega)\mu\nu} \right) \\ &+ \hat{\Gamma}_\rho(\hat{\rho}) \left(\bar{\Psi} \boldsymbol{\tau} \gamma_\mu \Psi A^{(\rho)\mu} + \frac{f_\rho}{m_\rho} \bar{\Psi} \sigma_{\mu\nu} \boldsymbol{\tau} \Psi F^{(\rho)\mu\nu} \right). \end{aligned} \quad (2.8)$$

A Lagrangian of the same type, but with bare coupling constants $\Gamma_\alpha(\rho) \rightarrow g_\alpha = \text{const.}$, is used for free-space NN scattering, serving to fix the bare coupling constants. The full set of mesons with the respective coupling constants is used to

obtain first the free space T matrix and the in-medium DB G matrix. As discussed in Ref. [19] the DBHF calculations are performed in asymmetric nuclear matter, making it possible to derive the full set of isoscalar and isovector self-energies. The self-energies contain via u -channel processes also pion and η -meson contributions. They are, in fact, important for a proper description of the density dependence of the self-energies. As discussed in Refs. [17–19], the self-energies are used to derive effective density-dependent Hartree vertices. Because, owing to parity, pseudoscalar mesons do not develop classical, condensed fields, neither the pion nor the η -meson fields contribute to the mean-field sector of the theory. They are, however, present in dynamical processes leading to excitations of the system. Here we are considering nuclear thermodynamics only on the mean-field level, thus leaving investigations of dynamical fluctuations to a future study. Hence, for the present work only the scalar and the vector interaction Lagrangians, Eqs. (2.7) and (2.8), respectively, will be of direct relevance once we have derived the DBHF vertices.

The Lagrangian of Eq. (2.1) is highly nonlinear in the fermionic field operators contained in the density operator $\hat{\rho}$. At the theoretical-mathematical level, this is a wanted property because it allows us to keep full control over all changes of the systems and imposes covariance of the field equations. The derivation of the vertex functionals and their explicit determination in mean-field approximation as functions of the density are discussed in Ref. [18].

With the standard Legendre transformation we obtain the DDRH energy momentum tensor $T^{\mu\nu}$ [17,20]. Of particular interest is the Hamiltonian density,

$$\begin{aligned} \mathcal{H} \equiv T^{00} &= \bar{\Psi}\gamma_0\Sigma^{(0)}\Psi + \bar{\Psi}(M - \Sigma^{s(0)})\Psi \\ &+ \sum_{\alpha=\sigma,\delta,\pi} \left\{ (\partial^0\phi_\alpha)^2 - \frac{1}{2}[\partial_\lambda\phi_\alpha\partial^\lambda\phi_\alpha - m_\alpha^2\phi_\alpha^2] \right\} \\ &+ \sum_{\alpha=\omega,\rho} \left\{ \partial^0 A_\lambda F^{(\alpha)\lambda 0} - \frac{1}{2}[m_\alpha^2 A_\mu^{(\alpha)} A^{\mu(\alpha)} - F_{\lambda\rho}^{(\alpha)} F^{\lambda\rho(\alpha)}] \right\}. \end{aligned} \quad (2.9)$$

The full energy momentum tensor $T^{\mu\nu}$ includes rearrangement contributions induced by the functional derivatives of the vertex functional [16–18], modifying, in particular, the pressure density $P \sim T^{ii}$.

By the standard techniques of finite-temperature quantum many-body theory [39], we introduce hadronic chemical potentials μ_q and the corresponding number operators N_q . Covariant thermodynamics are discussed below. Here we only indicate the connection to the more familiar nonrelativistic formulation. This is achieved by a canonical transformation

$$K = H - \sum_\eta \mu_\eta N_\eta, \quad (2.10)$$

from which the grand partition function is obtained,

$$Z_G = e^{-\beta\Omega} = \text{Tr} e^{-\beta K}, \quad (2.11)$$

and the statistical operator,

$$\rho_G = Z_G^{-1} e^{-\beta\Omega} = e^{-\beta(\Omega-K)}, \quad (2.12)$$

is serving to perform the thermodynamical average of observables over the grand-canonical ensemble. Explicit expression is derived below.

B. The DDRH field equations and mean-field approximation

From the above Lagrangian we derive by variation with respect to the Dirac-adjoint fermion field operators $\bar{\Psi}$ wave equations of Dirac type,

$$[\gamma_\mu(i\partial^\mu - \Sigma_\nu^\mu) - M - \Sigma_s]\Psi = 0. \quad (2.13)$$

They include the vector and scalar self-energies Σ_ν^μ and Σ_s , respectively [16]. The variation leads to two distinct types of self-energies,

$$\Sigma = \Sigma^{(b)} + \Sigma^{(r)}, \quad (2.14)$$

$$\Sigma^{(b)} = \frac{\partial \mathcal{L}_{\text{int}}}{\partial \bar{\Psi}}, \quad (2.15)$$

$$\Sigma^{(r)} = \frac{\partial \mathcal{L}_{\text{int}}}{\partial \hat{\rho}} \frac{\delta \hat{\rho}}{\delta \bar{\Psi}}. \quad (2.16)$$

The bare self-energies $\Sigma^{(b)}$ are of the conventional structure as also obtained in a theory with density-independent, constant vertices. Because our vertex functionals are derived from DB theory, they correspond to the standard DBHF self-energies [8,19]. The rearrangement self-energies $\Sigma^{(r)}$ in Eq. (2.16) represent an essential new feature of generic character for a density-dependent formalism. It is seen that these contributions originate from the variation of the vertex functionals, thus describing the response of interaction vertex on a change of the medium. Physically, $\Sigma^{(r)}$ accounts for the dynamical rearrangement effects of the nuclear medium by virtue of polarization [16,20].

The meson-field equations are given by the standard Klein-Gordan equations for the scalar and pseudoscalar fields,

$$(\partial_\mu\partial^\mu + m_\alpha^2)\Phi_\alpha = \hat{\Gamma}_\alpha(\hat{\rho})\bar{\Psi}\hat{O}_\alpha\Psi, \quad (2.17)$$

where $\hat{O}_\alpha \in \{1, \gamma_\mu, \gamma_5\} \otimes \{1, \tau\}$ and derivative terms may contribute as well. The vector fields obey the Proca equation,

$$\partial_\mu F^{(\alpha)\mu\nu} + m_\alpha^2 A^\nu = \hat{\Gamma}_\alpha(\hat{\rho})\bar{\Psi}\hat{J}_\alpha^\nu\Psi, \quad (2.18)$$

where $\bar{\Psi}\hat{J}_\alpha^\nu\Psi$ denotes the corresponding vector current. The only difference is that the vertices depend now on the background medium. For our purpose, the Bose fields are far off their mass shell. They are virtual fields which are fully determined by their nucleonic sources, contributing only in t - and u -channel processes among nucleons.

The field equations are to be solved for a given nuclear-matter ground-state configuration. Using the mean-field approximation we specify the expectation values of the functionals. Let $\rho = \langle \hat{\rho} \rangle$ be the ground-state expectation value of the operator $\hat{\rho} = \hat{\rho}(\bar{\Psi}_q, \Psi_q)$, which is a Lorentz-scalar functional of the proton and neutron, respectively, field operators Ψ_q . Using $\hat{\rho} = \rho + \delta\rho$ we expand the vertex functionals according to

$$\Gamma_\alpha(\rho + \delta\rho) = \Gamma_\alpha(\rho) + \left. \frac{\partial \Gamma_\alpha(\hat{\rho})}{\partial \hat{\rho}} \right|_\rho \delta\rho + \dots \quad (2.19)$$

Taking the ground-state expectation value of the vertex, the first-order correction $\delta\rho = \hat{\rho} - \rho$ vanishes identically, The first non-vanishing correction is given by

$$C(\hat{\rho}) = \langle (\hat{\rho} - \rho)^2 \rangle = \langle \hat{\rho}^2 \rangle - \rho^2, \quad (2.20)$$

determined by the quantal fluctuations of $\hat{\rho}$ with respect to the reference value ρ . In ground-state calculation we neglect terms of this and higher order consistently. Therefore, in nuclear matter the meson-field equations are always determined by source terms with a strength given by $\Gamma_\alpha(\rho)$, which is a number given as a function of ρ .

Thus, neglecting consistently all nonstationary fluctuations around the ground-state expectation values, we obtain the mean-field equations

$$(\vec{\nabla}^2 - m_\alpha^2)\Phi_\alpha = -\Gamma_\alpha(\rho)\langle\bar{\Psi}\mathcal{O}_{(\alpha)}\Psi\rangle, \quad (2.21)$$

$$(\vec{\nabla}^2 - m_\alpha^2)A^{(\alpha)\mu} = \Gamma_\alpha(\rho)\langle\bar{\Psi}\mathcal{O}^{(\alpha)\mu}\Psi\rangle, \quad (2.22)$$

where the fields are now classical scalar and vector fields, respectively.

In the following we apply the mean-field approximation to the full Lagrangian, Eq. (2.1). As a consequence of time-reversal invariance and parity conservation, the pseudoscalar and pseudovector fields will become identical to zero in the ground state. However, there is still an implicit contribution of these fields to the of the remaining density-dependent couplings, because they are derived from the full DB theory. This can be seen with the help of the Fierz transformation and decomposition of the exchange diagrams in terms of direct channels. [19].

As already indicated in the previous section, we use the DDRH theory in mean-field approximation, with the explicit inclusion of the σ , δ , ω , and ρ meson mean fields. The interaction part of the Lagrangian then simplifies to

$$\begin{aligned} \mathcal{L}_{\text{int}} = & \Gamma_\sigma(\rho)\bar{\Psi}\Phi_\sigma\Psi + \Gamma_\delta(\rho)\bar{\Psi}\boldsymbol{\tau}\Phi_\delta\Psi - \Gamma_\omega(\rho)\bar{\Psi}\gamma_\mu A^{(\omega)\mu}\Psi \\ & - \Gamma_\rho(\rho)\bar{\Psi}\boldsymbol{\gamma}\boldsymbol{\tau}A^{(\rho)\mu}. \end{aligned} \quad (2.23)$$

The first derivative terms in Eq. (2.19) lead to the mean-field rearrangement self-energies, including scalar and vector components:

$$\Sigma^{s(r)} = \sum_\alpha \left(\frac{\partial\Gamma_\alpha}{\partial\hat{\rho}} \Big|_\rho \langle\bar{\Psi}\mathcal{O}_\alpha\Psi\rangle \Phi_\alpha \right), \quad (2.24)$$

$$\Sigma^{v(r)} = \sum_\alpha \left(\frac{\partial\Gamma_\alpha}{\partial\hat{\rho}} \Big|_\rho \langle\bar{\Psi}\mathcal{O}_\mu^{(\alpha)}\Psi\rangle A^{(\alpha)\mu} \right). \quad (2.25)$$

The self-energies are decomposed into isoscalar and isovector parts,

$$\begin{aligned} \hat{\Sigma}^{s(0)} &= \hat{\Gamma}_\sigma(\hat{\rho})\phi_\sigma + \hat{\Gamma}_\delta(\hat{\rho})\boldsymbol{\tau} \cdot \boldsymbol{\Phi}_\delta \\ &= \hat{\Sigma}_0^{s(0)} + \boldsymbol{\tau} \hat{\Sigma}_1^{s(0)}, \end{aligned} \quad (2.26)$$

and correspondingly, for the vector self-energies,

$$\begin{aligned} \hat{\Sigma}^{\mu(0)} &= \hat{\Gamma}_\rho(\hat{\rho})A^{(\omega)\mu} + \hat{\Gamma}_\rho(\hat{\rho})\boldsymbol{\tau} \cdot A^{(\rho)\mu} \\ &= \hat{\Sigma}_0^{(0)\mu} + \boldsymbol{\tau} \hat{\Sigma}_1^{(0)\mu}, \end{aligned} \quad (2.27)$$

where we have left out the photon field. For infinite nuclear matter we find explicitly in Hartree approximation [18] the

nonvanishing self-energies

$$\begin{aligned} \Sigma_q^{s(0)}(\hat{\rho}) &= \Gamma_\sigma(\hat{\rho})\Phi_\sigma + \tau_q\Gamma_\delta(\hat{\rho})\Phi_\delta, \\ \Sigma_q^{0(0)}(\hat{\rho}) &= \Gamma_\omega(\rho)A_0^{(\omega)} + \tau_q\Gamma_\rho(\hat{\rho})A_0^{(\rho)}, \\ \Sigma^{0(r)}(\hat{\rho}) &= \frac{\partial\Gamma_\omega}{\partial\hat{\rho}}A_0^{(\omega)}\rho_0 + \frac{\partial\Gamma_\rho}{\partial\hat{\rho}}A_0^{(\rho)}\rho_1 - \frac{\partial\Gamma_\sigma}{\partial\hat{\rho}}\Phi_\sigma\rho^s \\ &\quad - \frac{\partial\Gamma_\delta}{\partial\hat{\rho}}\Phi_\delta\rho_1^s, \end{aligned} \quad (2.28)$$

where proton ($q = p$) and neutron ($q = n$) contributions are indicated and $\tau_q = \pm 1$ denotes the corresponding expectation values of the isospin τ_3 operator, respectively. All vertex derivatives are to be evaluated at $\hat{\rho} = \rho$. Because isospin symmetry requires that the vertices must depend only on isoscalar quantities the rearrangement self-energies do not depend on the nucleonic charge state. Defining the proton and neutron vector densities by $\rho_q = \langle 0|\bar{\Psi}_q\boldsymbol{\gamma}_0\Psi_q|0\rangle$ and similarly the corresponding scalar densities by $\rho_q^s = \langle 0|\bar{\Psi}_q\Psi_q|0\rangle$, we find the isoscalar ($I = 0$) and isovector ($I = 1$) vector and scalar densities, respectively,

$$\rho_I = \rho_n + (-)^I\rho_p, \quad (2.29)$$

$$\rho_I^s = \rho_n^s + (-)^I\rho_p^s. \quad (2.30)$$

It can be easily verified that in Eq. (2.28) the isovector pieces are, in fact, of quadratic order in ρ_1 and ρ_1^s , respectively.

The proton and neutron wave functions, respectively, obey Dirac equations of standard form,

$$[\boldsymbol{\gamma}_\mu(i\partial^\mu - \hat{\Sigma}_q^\mu) - (M_q - \hat{\Sigma}_q^s)]\Psi_q = 0, \quad (2.31)$$

but with the self-energies as defined as in Eq. (2.14) and constructed by means of the results in Eq. (2.28).

Because we include interactions in the scalar-isovector channel represented by the $\delta/a_0(980)$ meson, the effective mass of the nucleons is explicitly isospin dependent in DDRH theory [18,19],

$$M_q^* = M - \Gamma(\rho)\phi_\sigma - \tau_q\Gamma_\delta(\rho)\phi_\delta. \quad (2.32)$$

III. THERMODYNAMICS OF NUCLEAR MATTER

A. Covariant thermodynamics

In the covariant formulation of thermodynamics it is expedient to express all equations in terms of Lorentz scalars and Lorentz four-vectors. For this purpose we follow the steps from Ref. [5] by introducing the thermal potential $\alpha = \beta\mu$ and the thermal timelike four-vector $\beta_\mu = \beta u^\mu$, where $u^\mu = \frac{1}{\sqrt{1-v^2/c^2}}(1, \mathbf{v})$ is the fluid velocity four-vector and $\beta = 1/T$ the inverse temperature.

A system of a set of conserved currents j_c^μ in equilibrium is described by the energy momentum tensor $T^{\mu\nu}$ and the entropy flux σ^μ . These quantities are connected by the first law of thermodynamics [28,40],

$$\beta_\nu dT^{\nu\mu} = d\sigma^\mu + \sum_c \alpha_c dj_c^\mu. \quad (3.1)$$

The pressure P can be expressed in terms of the primary functions by

$$P\beta^\mu = -\beta_\nu T^{\nu\mu} + \sigma^\mu + \sum_c \alpha_c j_c^\mu. \quad (3.2)$$

In statistical quantum mechanics, the thermodynamic functions are related to ensemble averages of quantum-mechanical operators. This is usually achieved by defining a grand partition function Z and a corresponding four-vector potential $\Phi^\mu(\alpha_c, \beta_\nu)$. The partition function is

$$Z \equiv \text{Tr} \left\{ \exp \left(\int d\mathcal{F}_\mu \left[\sum_c \alpha_c j_c^\mu - \beta_\nu T^{\nu\mu} \right] \right) \right\}, \quad (3.3)$$

where \mathcal{F}_μ denotes the four-dimensional infinitesimal surface element. By varying β_ν and α_c one can derive a differential equation that connects Φ^μ with the energy momentum tensor and the conserved currents,

$$d\Phi^\mu = T^{\mu\nu} d\beta_\nu - \sum_c j_c^\mu d\alpha_c, \quad (3.4)$$

providing the covariant thermodynamic laws

$$T^{\mu\nu} = \left(\frac{\partial \Phi^\mu}{\partial \beta_\nu} \right)_{\alpha_c}, \quad (3.5a)$$

$$j_{c'}^\mu = - \left(\frac{\partial \Phi^\mu}{\partial \alpha_{c'}} \right)_{\beta_\nu, \alpha_c, c \neq c'}. \quad (3.5b)$$

Furthermore, after differentiating Eq. (3.2) and using the first law of thermodynamics, Eq. (3.1), we arrive at the covariant form of the Gibbs relation:

$$\Phi^\mu = -P\beta^\mu = \beta_\nu T^{\nu\mu} - \sigma^\mu - \sum_c \alpha_c j_c^\mu. \quad (3.6)$$

In the comoving frame $u^\mu = (1, 0, 0, 0)$, thus, Eq. (3.3) reduces to

$$Z \equiv \sum_n \langle n | e^{-\beta(\hat{H} - \sum_c \mu_c \hat{N}_c)} | n \rangle = \text{Tr} e^{-\beta(\hat{H} - \sum_c \mu_c \hat{N}_c)}, \quad (3.7)$$

where \hat{H} is the Hamiltonian describing the system and \hat{N}_c the number operator. In Eq. (3.7) the trace has to be taken as a sum over all energy and particle eigenstates $|n\rangle$. With this, the above expressions lead to a connection between the thermodynamic potential and other thermodynamic functionals:

$$\Phi^\mu(\alpha_c, \beta_\nu) = -\frac{1}{V} \ln Z u^\mu = \frac{\Omega(T, \mu, V)}{TV} u^\mu, \quad (3.8a)$$

$$\rho_c = -\frac{1}{V} \frac{\partial \Omega}{\partial \mu_c}, \quad (3.8b)$$

$$S = \beta \left(\mathcal{E} - \Omega - \sum_b \mu_b \rho_b \right). \quad (3.8c)$$

According to the HVH theorem [23], the thermodynamic and the hydrostatic pressure must coincide, i.e.,

$$P = \rho^2 \frac{\partial \mathcal{F}}{\partial \rho} = \frac{1}{3} \sum_{i=1}^3 \langle T^{ii} \rangle, \quad (3.9)$$

with the free energy $\mathcal{F} = \mathcal{E}/\rho - TS$. In Eq. (3.9) the thermal average is used, which for an arbitrary operator \hat{O} is given by the prescription

$$\langle \hat{O} \rangle = \frac{\text{Tr}[e^{\beta(\hat{H} - \sum_c \mu_c \hat{N}_c)} \hat{O}]}{\text{Tr}[e^{\beta(\hat{H} - \sum_c \mu_c \hat{N}_c)}]} = \text{Tr}[\hat{\rho} \hat{O}]. \quad (3.10)$$

Consider now the DDRH Hamilton operator, which in mean-field approximation (MFA) is given by

$$\begin{aligned} \hat{H}(\hat{\rho}) = T^{00} = & \left(\sum_b \bar{\psi}_b \{ i\gamma \nabla + \gamma_0 \Sigma_b^{0(0)}(\hat{\rho}) + [M - \Sigma_b^S(\hat{\rho})] \} \right. \\ & \times \psi_b + \frac{1}{2} m_\sigma^2 \phi_\sigma^2 + \frac{1}{2} m_\delta^2 \phi_\delta^2 - \frac{1}{2} m_\omega^2 A_0^{(\omega)2} \\ & \left. - \frac{1}{2} m_\rho^2 A_0^{(\rho)2} \right), \end{aligned} \quad (3.11)$$

where the sum over b includes all baryons considered in the model. An important consequence of the MFA is the cancellation of the rearrangement term in the Hamiltonian. However, because the interaction vertices are functionals of the density operator, $\hat{\rho}$ the calculation of the partition function (3.7) needs to be examined carefully. To derive Z , it is necessary to evaluate a trace over the eigenstates in Fock space. This is only possible if the exponential function can be decomposed into a sum of independent terms. To fulfill this requirement in the DDRH model, the Hamiltonian should be approximated by a one-body operator. For this purpose the density-dependent interaction vertices $\hat{\Gamma}_{b\alpha}$ are expanded around the thermal equilibrium density mean value $\rho_0 = \langle \hat{\rho} \rangle$, keeping only terms up to the first order in $(\hat{\rho} - \rho_0)$ [see also Eq. (2.19)]

$$\Gamma_\alpha(\hat{\rho}) = \Gamma_\alpha(\rho_0) + \left. \frac{\partial \Gamma_\alpha}{\partial \hat{\rho}} \right|_{\hat{\rho}=\rho_0} (\hat{\rho} - \rho_0) + \mathcal{O}[(\hat{\rho} - \rho_0)^2].$$

With this assumption the expectation values of the vertex functionals become functions of the density, i.e., $\langle \hat{\Gamma}(\hat{\rho}) \rangle \rightarrow \Gamma(\rho_0)$. Hence, the Hartree vertices are now implicitly temperature dependent, $\Gamma(\rho, T) = \Gamma[\rho(T)]$. However, this approach implies an expansion for the Hamilton operator

$$H(\hat{\rho}) = H^0(\rho_0) + H^R(\hat{\rho}),$$

with

$$\begin{aligned} H^R(\hat{\rho}) = & \Sigma^{(r)}(\rho_0)(\hat{\rho} - \rho_0) \\ = & \sum_b \left(\left. \frac{\partial \Gamma_{b\sigma}}{\partial \hat{\rho}} \right|_{\hat{\rho}=\rho_0} \phi_\sigma \rho_b^s + \left. \frac{\partial \Gamma_{b\delta}}{\partial \hat{\rho}} \right|_{\hat{\rho}=\rho_0} \phi_\delta \tau_b^3 \rho_b^s \right. \\ & \left. + \left. \frac{\partial \Gamma_{b\omega}}{\partial \hat{\rho}} \right|_{\hat{\rho}=\rho_0} A_\omega^0 \rho_b + \left. \frac{\partial \Gamma_{b\rho}}{\partial \hat{\rho}} \right|_{\hat{\rho}=\rho_0} A_\rho^0 \tau_b^3 \rho_b \right) (\hat{\rho} - \rho_0). \end{aligned} \quad (3.12)$$

This shows that the in-medium correlations described by the density-dependent couplings indeed are inducing a rearrangement perturbation in the Hamilton operator. Given this approximation, all operators in the exponential of the partition function are now diagonal. This makes an exact calculation feasible. From the stationary solution of the Dirac equation in

MFA, we find the energies for baryons and antibaryons at the equilibrium nuclear-matter density ρ_0 ,

$$\varepsilon_b^\pm(k) = \pm E_b^*(k) + \Sigma_b^{0(0)} + \Sigma^{(r)}(\rho_0), \quad (3.13)$$

with $E_b^*(k) = \sqrt{k^2 + M_b^{*2}}$. Considering the normal ordered products of the baryon fields, we can now go through the usual steps for the calculation of the partition function. Indeed, introducing effective baryon masses and effective chemical potentials as

$$\begin{aligned} M_b^* &\equiv M_b - \Sigma_b^S, \\ \nu_b &\equiv \mu - \Sigma_b^0 = \mu - \Sigma_b^{0(0)} - \Sigma^{(r)}, \end{aligned} \quad (3.14)$$

leads to the same expression for the baryonic part of the thermodynamic potential as in the noninteracting case. This time, however, the baryon masses and the chemical potentials are replaced by their effective values. Because the meson fields are treated as classical fields, their contribution to the partition function is trivial. Thus, we can split Φ^μ into a baryon, a mean-field, and a rearrangement part,

$$\Phi^\mu = \sum_b \Phi_b^\mu + \Phi_{\text{MF}}^\mu + \Phi_{\text{R}}^\mu, \quad (3.15)$$

with

$$\begin{aligned} \Phi_b^\mu &= - \sum_s \int \frac{d^3k}{(2\pi)^3} [\ln(1 + e^{-\beta(E_k^* - \nu_b)}) \\ &\quad + \ln(1 + e^{-\beta(E_k^* + \nu_b)})] u^\mu, \end{aligned} \quad (3.16)$$

$$\Phi_{\text{MF}}^\mu = \beta \left(\frac{1}{2} m_\sigma^2 \phi_\sigma^2 + \frac{1}{2} m_\delta^2 \phi_\delta^2 - \frac{1}{2} m_\omega^2 A_0^{(\omega)2} - \frac{1}{2} m_\rho^2 A_0^{(\rho)2} \right) u^\mu, \quad (3.17)$$

$$\Phi_{\text{R}}^\mu = -\beta \rho_0 \Sigma_0^{(r)} u^\mu. \quad (3.18)$$

The fluctuations around the equilibrium density coming from density-dependent correlations show up as rearrangement terms in Φ_{R}^μ . Consequently, the pressure $P = -\Phi^0/\beta^0$ is also modified by additional rearrangement contributions, which are crucial to fulfill the HVH theorem. However, the rearrangement parts cancel out in the entropy and energy density. For the latter, for example, this can be verified by applying Eq. (3.5a) to Φ^μ ,

$$\begin{aligned} \mathcal{E} &= \left. \frac{\partial \Phi^0}{\partial \beta^0} \right|_{\alpha_b} \\ &= \sum_b \left\{ 2 \int \frac{d^3k}{(2\pi)^3} E_k^* [f_B(\nu_b) + \bar{f}_B(\nu_b)] + \Sigma_b^{0(0)} \rho_b \right\} \\ &\quad + \frac{1}{2} \left(\sum_{s=\sigma,\delta} m_s^2 \Phi_s^2 - \sum_{v=\omega,\rho} m_v^2 A_0^{v2} \right). \end{aligned} \quad (3.19)$$

Note that in the calculation of the above derivative all parameters $\alpha_b = \beta \mu_b$ have to be held fixed.

In thermal equilibrium the meson fields should be chosen such that they minimize Φ^μ , i.e., $(\frac{\partial \Omega}{\partial \chi})_{\beta, \mu_b} = 0$ for $\chi \in$

$\{\phi_\sigma, \phi_\delta, A_0^\omega, A_0^\rho\}$. This results in the following equations:

$$\begin{aligned} \phi_\sigma &= \sum_b \frac{\Gamma_{b\sigma}}{m_\sigma^2} \rho_b^s \equiv \sum_b \frac{\Gamma_{b\sigma}}{m_\sigma^2} 2 \int \frac{d^3k}{(2\pi)^3} \frac{M_b^*}{E_b^*} \\ &\quad \times [f_B(\nu_b, T) + \bar{f}_B(\nu_b, T)], \end{aligned} \quad (3.20a)$$

$$\begin{aligned} \phi_\delta &= \sum_b \frac{\Gamma_{b\delta}}{m_\delta^2} \rho_b^{s(3)} \equiv \sum_b \frac{\Gamma_{b\delta}}{m_\delta^2} 2\tau_b^3 \int \frac{d^3k}{(2\pi)^3} \frac{M_b^*}{E_b^*} \\ &\quad \times [f_b(\nu_b, T) + \bar{f}_B(\nu_b, T)], \end{aligned} \quad (3.20b)$$

$$\begin{aligned} A_0^\omega &= \sum_b \frac{\Gamma_{b\omega}}{m_\omega^2} \rho_b \equiv \sum_b \frac{\Gamma_{b\omega}}{m_\omega^2} 2 \int \frac{d^3k}{(2\pi)^3} \\ &\quad \times [f_B(\nu_b, T) - \bar{f}_B(\nu_b, T)], \end{aligned} \quad (3.20c)$$

$$\begin{aligned} A_0^\rho &= \sum_b \frac{\Gamma_{b\rho}}{m_\rho^2} \rho_b^3 \equiv \sum_b \frac{\Gamma_{b\rho}}{m_\rho^2} 2\tau_b^3 \int \frac{d^3k}{(2\pi)^3} \\ &\quad \times [f_B(\nu_b, T) - \bar{f}_B(\nu_b, T)]. \end{aligned} \quad (3.20d)$$

In the limit of $T \rightarrow 0$ the particle distribution function becomes the well-known step function, $f_B(\nu_b) \rightarrow \Theta(\nu_b - E_k^*) \equiv \Theta(k_{F_b} - k)$, while the antiparticle distribution function \bar{f}_B vanishes completely. This defines the Fermi momenta and Fermi energies of the baryons as $\nu_b = E_{F_b}^* = \sqrt{k_{F_b}^2 + M_b^{*2}}$. The solution of the baryon densities and, accordingly, the vector meson fields becomes trivial for vanishing T , while the scalar densities can be found by a self-consistent solution of the transcendental equation

$$\rho_b^s = \frac{M_b^*}{2\pi^2} \left(E_{F_b}^* k_{F_b} - M_{F_b}^{*2} \ln \left[\frac{E_{F_b}^* + k_{F_b}}{M_b^*} \right] \right). \quad (3.21)$$

The energy density and pressure of cold nuclear matter are then given by

$$\begin{aligned} \mathcal{E}(T=0) &= \sum_b \frac{1}{4} (3E_{F_b} \rho_b + M_b^* \rho_b^s) \\ &\quad + \sum_b \frac{1}{2} (\rho_b \Sigma^{0(0)b} + \rho_b^s \Sigma_b^S), \end{aligned} \quad (3.22)$$

$$\begin{aligned} P(T=0) &= \frac{1}{4} \sum_b (E_{F_b} \rho_b - M_b^* \rho_b^s) \\ &\quad + \frac{1}{2} \sum_b (\rho_b \Sigma_b^{0(0)} - \rho_b^s \Sigma_b^S) + \rho \Sigma^{(r)}, \end{aligned} \quad (3.23)$$

where $\rho = \sum_b \rho_b$ is the total baryon density.

B. The density and temperature dependence of DDRH vertices and self-energies

Typically, nuclear-matter mean-field models assume tacitly that interactions are essentially unaffected by temperature. Already quite early, ter Haar and Malfliet [8] have addressed that question by means of finite-temperature DBHF calculations. They indeed find a weak temperature dependence of the resulting G -matrix interaction. A closer inspection of the DB equations at $T > 0$ reveals the reason for that behavior.

The medium and temperature dependence of the G matrix is introduced by two sources, namely the Pauli blocking of

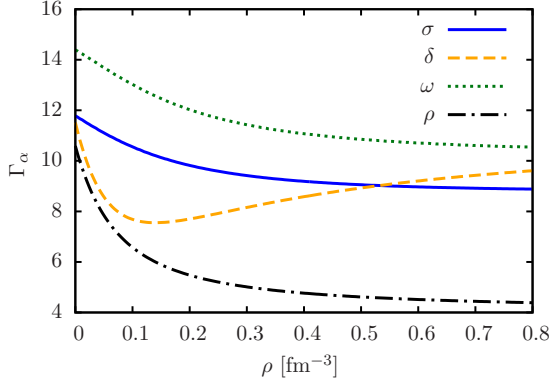


FIG. 1. (Color online) Density dependence of the DDRH nucleon-meson vertices at $T = 0$ [18].

the Fermi sphere of occupied single-particle states and the baryon self-energies. In leading order, contributions from the Pauli principle, i.e., Fermi statistics, are dominant. Therefore, preparatory to the discussion of the EOS, we should take a closer look at the DDRH vertices first. In Fig. 1 the density dependence of the DDRH vertices is shown. One can nicely see that the density dependence has its most impact in the lower density region and becomes less significant for $\rho > 0.5 \text{ fm}^{-3}$. Basically, this circumstance arises from the fact that in the high-density region the contributions from intrinsic particle fluctuations are small compared to the ones coming from the occupied Fermi sea states. The functional behavior of the δ -meson vertex differs considerably from the one of the other mesons. While all other vertices constantly fall off with rising ρ the δ -meson vertex shows a special functional behavior with a minimum at $\rho \approx 0.14 \text{ fm}^{-3}$. The inclusion of this channel is a key feature of the DDRH model, which leads to a splitting of the effective nucleon masses in asymmetric nuclear matter, as discussed later. The DDRH vertices are deduced from comparing the DDRH potential energy with the Brueckner calculations [17,18]. In general, the proper DB self-energies, Σ^{DB} , are momentum dependent, while the DDRH self-energies are not, because they are calculated in the MFA. The usual approach to map $\Sigma^{\text{DDRH}}(\rho, T)$ on $\Sigma^{\text{DB}}(k, \rho, T)$ is to calculate the average of Σ^{DB} over the Fermi sea. For the vector self-energies this implies

$$\begin{aligned} \Sigma_{\alpha}^{\text{DDRH}}(\rho, T) &= \rho \frac{\Gamma_{\alpha}^2}{m_{\alpha}^2} \\ &= \frac{4}{(2\pi)^3} \frac{1}{\rho} \int d^3k \Sigma_{\alpha}^{\text{DB}}(k, \rho, T) (f_B - \bar{f}_B). \end{aligned} \quad (3.24)$$

For scalar self-energies ρ has to be replaced with ρ_s on the left-hand side of (3.24).

In Ref. [19] it was shown that the DB self-energies can be approximated by quadratic functions in the momentum k in the vicinity of the Fermi momentum k_F . Hence, an expansion of Σ^{DB} up to the first order in k^2 around the Fermi momentum is necessary and sufficient to reproduce the DB EOS properly,

$$\Sigma^{\text{DB}}(k, \rho) \approx \Sigma_F^{\text{DB}}(\rho) + (k^2 - k_F^2) \Sigma_F^{\prime \text{DB}}(\rho), \quad (3.25)$$

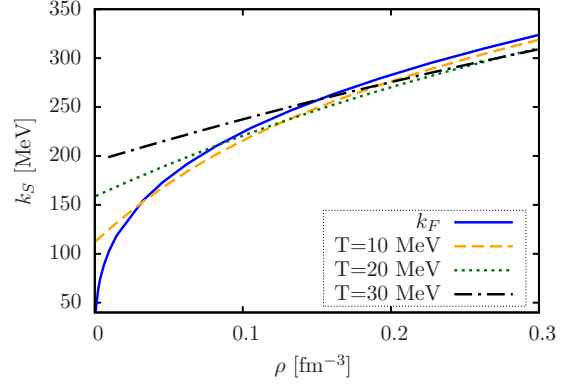


FIG. 2. (Color online) Comparison of k_S versus the Fermi momentum k_F for $T = 10, 20,$ and 30 MeV .

with the definitions $\Sigma_F^{\text{DB}} = \Sigma^{\text{DB}}(k_F, \rho)$, $\Sigma_F^{\prime \text{DB}} = \frac{\partial \Sigma^{\text{DB}}(k, \rho)}{\partial k} \Big|_{k=k_F}$. The Fermi momentum k_F is given by the relation $\sqrt{k_F^2 + M^{*2}} = \nu$ at $T = 0$. Thus, k_F is not well defined for $T > 0$ and should be replaced with a more suitable quantity at finite T . One possibility is to define the momentum k_S , where the Fermi distribution is half its value at $k = 0$,

$$f_B(k_S, T, \nu) = \frac{1}{2} f_B(0, T, \nu).$$

Because the weight factor $k^2 f_B(k, T, \nu)$ in the momentum integral peaks near k_S , it is useful to evaluate Σ^{DB} around this momentum value instead. Because $k_S \rightarrow k_F$ for $T \rightarrow 0$, this definition is compatible with zero-temperature calculations. In Fig. 2 k_S is plotted as a function of ρ for some temperature values. One can see that there is only a significant difference at low densities and high temperatures between k_S and k_F . The differences between $\Sigma^{\text{DB}}(k_S)$ and $\Sigma^{\text{DB}}(k_F)$ are very small in this region. This was also found by ter Haar and Malfliet in Ref. [7]. Nevertheless, we substitute k_F with k_S in Eq. (3.25) from now on to provide a well-defined expansion scheme for all temperatures. In the range of moderate temperatures the DB self-energies show a very small temperature dependence [7,41]. As an example, Fig. 3 illustrates the temperature dependence of Σ^{DB} as obtained by Ref. [7]. From this we conclude that it is not only possible to apply the same

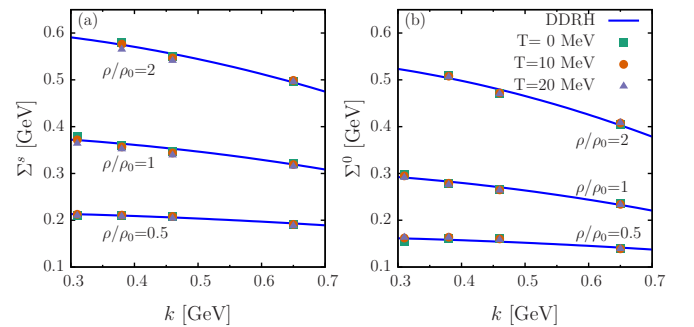


FIG. 3. (Color online) The real part of the scalar (a) and vector (b) DB self-energies at different temperatures and densities [8], compared to the quadratic approximation discussed in the text.

quadratic expansion of Σ^{DB} , as suggested by Ref. [19] at $T > 0$, but even to neglect the temperature dependence of the self-energies in a first-order approximation. Substituting Σ^{DB} with Eq. (3.25) in Eq. (3.24) gives the following expression for the momentum-corrected DDRH vertices:

$$\begin{aligned} \Gamma_\alpha^2 &= \frac{4m_\alpha^2}{(2\pi)^3} \frac{1}{\rho_\alpha} \Sigma_S \left[1 + \frac{\Sigma'_S}{\Sigma_S} \frac{1}{\rho} \int d^3k (k^2 - k_S^2) (f_B - \bar{f}_B) \right] \\ &\equiv \Gamma_{(0)\alpha}^2 (1 + C_S^\alpha I_M). \end{aligned} \quad (3.26)$$

In Eq. (3.26) ρ_α corresponds to ρ and ρ_s for vector and scalar mesons, respectively. $\Gamma_{(0)\alpha}$ is the first-order approximation to the dressed vertex, including only Hartree contributions from DB self-energies. For vector mesons $\Gamma_{(0)\alpha}$ is density dependent, while for scalar mesons it additionally depends on the temperature, because ρ_s is a function of T at fixed ρ . In this case we can further separate $\Gamma_{(0)s}$,

$$\Gamma_{(0)s}(\rho, T) = \tilde{\Gamma}_{(0)s}(\rho) \sqrt{\frac{\rho_s(T=0)}{\rho_s(T)}} \equiv \tilde{\Gamma}_{(0)s}(\rho) I_s(\rho, T). \quad (3.27)$$

Obviously, $\Gamma_{(0)s}(T=0) = \tilde{\Gamma}_{(0)s}$. The function I_s provides an additional temperature correction to the scalar vertex. It is important to note here that a modification of Γ_s causes a modification of ρ_s , which, in turn, implies a different value for Γ_s . Therefore, $I_s(\rho, T)$ must be calculated numerically by solving the self-consistency problem.

The second term in Eq. (3.26) incorporates momentum corrections to the vertex, where $C_S^\alpha = \Sigma'_S / \Sigma_S$ and the momentum integral I_M is given by

$$I_M(\rho, T) = \frac{2}{\pi^2 \rho} \int dk k^2 [k^2 - k_S^2(T)] [f_B(T) - \bar{f}_B(T)].$$

As already mentioned, the parameter C_S can be assumed as independent of density and temperature. However, the momentum integral depends explicitly on both, ρ and T ,

$$I_M = I_M(\rho, T).$$

At $T = 0$ the expression for Γ_α^2 simplifies to

$$\begin{aligned} \Gamma_\alpha^2(\rho, T=0) &= \tilde{\Gamma}_{(0)\alpha}^2 \left[1 + C_S^\alpha \frac{2}{\pi^2 \rho} \left(-\frac{2}{15} k_F^5 \right) \right] \\ &= \tilde{\Gamma}_{(0)\alpha}^2 \left[1 - \frac{2}{5} C_S^\alpha k_F^2 \right] = \tilde{\Gamma}_{(0)\alpha}^2 [1 - \kappa C_S^\alpha \rho^{2/3}], \end{aligned} \quad (3.28)$$

with $\kappa = \frac{2}{5} \left(\frac{3}{2} \pi^2 \right)^{\frac{2}{3}}$.

As thermal excitations become important with increasing T , the momentum correction integral I_M will considerably differ from $\kappa \rho^{\frac{2}{3}}$. The constant factor κC_S^α , however, turns out to be very small, leading to a modification of the scalar and vector couplings by only 0.8% and 0.1%, respectively [18]. Therefore, the temperature dependence of Γ_α induced by I_M remains small in the temperature and density ranges relevant for this work. For further discussion, we introduce the

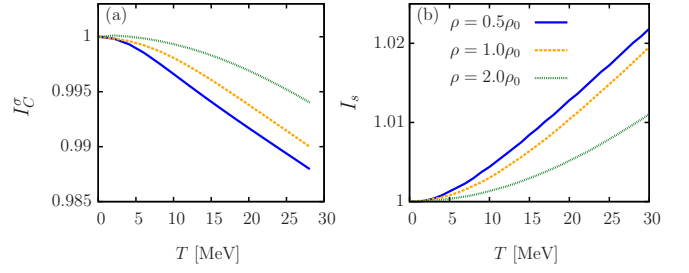


FIG. 4. (Color online) Temperature dependence of the scalar coupling functions I_C^σ (a) and I_s^σ (b) at different densities: $\rho = 0.5\rho_0$ (blue line), $\rho = \rho_0$ (orange dashed line), $\rho = 2\rho_0$ (green dotted line), where ρ_0 is the saturation density at $T = 0$. Lower curves belong to lower densities.

function I_C^α ,

$$I_C^\alpha(\rho, T) \equiv \left\{ \frac{[1 + C_S^\alpha I_M(T)]}{[1 + C_S^\alpha I_M(T=0)]} \right\}^{\frac{1}{2}}, \quad (3.29)$$

which describes the temperature-dependent correction factor on Γ_α arising from the momentum correction integral. This gives the following separation ansatz for Γ_α :

$$\Gamma^\alpha = \Gamma^\alpha(T=0) I_C^\alpha(T) I_s^\alpha(T). \quad (3.30)$$

Note that $I_s = 1$ for vector mesons.

In Fig. 4 the functions $I_C^\sigma(T)$ and $I_s^\sigma(T)$ for the σ -meson coupling are shown at various densities ρ . First of all, we see that the temperature dependence becomes less significant with increasing ρ . As expected, the momentum correction integral results in small deviations of Γ_σ from its zero-temperature value. While I_C^σ falls off continuously with rising T the scalar correction function I_s^σ shows an opposite behavior. Thus, the two effects partially compensate each other. In the range of moderate temperatures, where the liquid-gas phase transition takes place, the net correction is less than 0.5% and it stays small even at higher T . For the vector coupling Γ_ω we find that the corrections are even less than 0.2%.

This analysis therefore shows that the approximation

$$\Gamma^{\text{DDRH}}(\rho, T) \approx \Gamma^{\text{DDRH}}(\rho, T=0) \quad (3.31)$$

can be applied for the DDRH vertices. The temperature-dependent corrections would have nearly negligible small effects on the finite-temperature EOS for temperatures below 100 MeV. Besides, there are only few experimental data available for warm nuclear matter and it comes with large uncertainties as in the case of liquid-gas critical temperature, for example [42]. Hence, we use the effective vertices in first-order approximation, assuming a density dependence only. Within this approximation our calculations are in very good agreement with other models, as shown below. The temperature-dependent momentum corrections can be used in future calculations to fine tune the EOS properties, whenever more precise data will be available.

In the temperature range considered here, $T < 100$ MeV, the Fermi-Dirac statistics is exerting only little or, at best, a moderate influence on the G matrix. Most of the high-energy tails of the thermal distributions are suppressed by

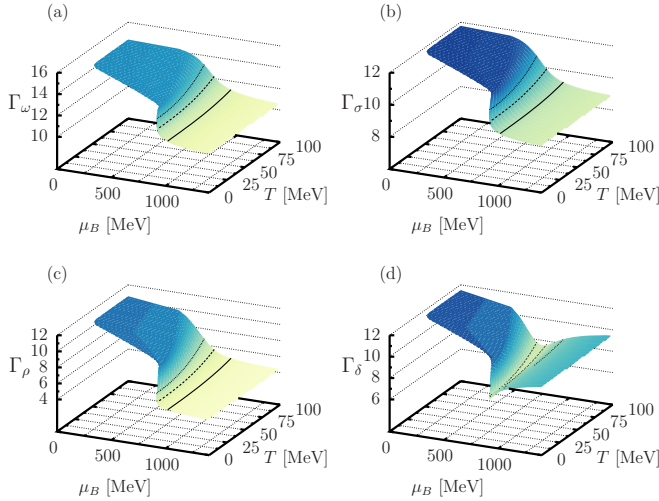


FIG. 5. (Color online) Dependence of the Hartree mean-field vertices on chemical potential and temperature in symmetric nuclear matter. Results for the vector vertices (ω, ρ) and the scalar vertices (σ, δ), respectively, are displayed in the left and the right columns, respectively. The dashed isolines indicate the constant density values of $0.5\rho_0$, ρ_0 , and $2\rho_0$.

the vertex form factors typically used to regularize the Bethe-Salpeter correlation integral. These expected properties are well reflected by our vertex functionals. The dependence of the vertices on chemical potential and temperature in Hartree approximation are illustrated in Fig. 5. The variations observed for high temperatures at chemical potentials close to the nucleon mass are corresponding to the increased polarizability of low-density nuclear matter. At these densities, the tails of the thermal distributions are not yet suppressed by the vertex form factors, hence leading to a stronger influence on the in-medium interactions. Note that the isolines in Fig. 5 correspond to constant nuclear-matter densities.

In other studies, the density dependence of the meson-baryon vertices has been determined in a phenomenological approach, where the functional form of the vertices is adjusted to fit measured properties of symmetric and asymmetric nuclear matter and spherical nuclei. The first phenomenological description was introduced by Typel and Wolter [38]. The parameters were further adjusted to calculations of giant multipole resonances in Refs. [43] and [24]. Thus, in the present work we compare the results of the DDRH model to those obtained with the phenomenological DD-ME2 parametrization of the vertices as given in Ref. [24]. To better understand the effects arising from density-dependent effective couplings, we also show some results for the linear Walecka model with constant couplings, which we refer to as QHD.

IV. EQUATION OF STATE FOR ISOSPIN-SYMMETRIC NUCLEAR MATTER

To begin with, we discuss our results for isospin-symmetric nuclear matter at $T > 0$. An important quantity in the analysis of nuclear many-body properties is the binding energy per

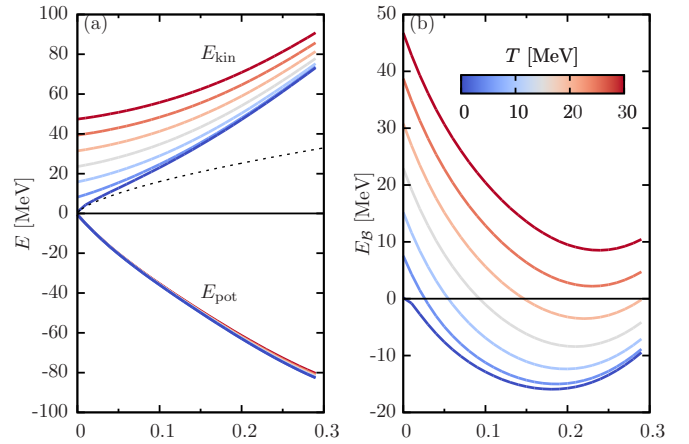


FIG. 6. (Color online) (a) Density dependence of the kinetic (upper curves), potential (lower curves). (b) Binding energy per particle within the DDRH approach. Isotherms for temperatures $T = 0$ MeV to $T = 30$ MeV in equidistant steps of 5 MeV are displayed. Note that lower curves correspond to lower temperatures.

nucleon,

$$E_B = \frac{\mathcal{E}}{\rho} - M, \quad (4.1)$$

with the total baryon density $\rho = \sum_b \rho_b$ and $M = \sum_b \frac{\rho_b}{\rho} M_b$. For the analysis of the different many-body effects it is helpful to separate E_B in a kinetic and a potential part; i.e., $E_B = E_{\text{kin}} + E_{\text{pot}}$. By inserting \mathcal{E} from Eq. (3.19) into the above equation and expressing the meson fields with the help of the corresponding self-energies, we can write

$$E_{\text{kin}} = \frac{2}{\rho} \sum_b \left[\int \frac{d^3k}{(2\pi)^3} E^*(f_B + \bar{f}_B) - M_b^* \rho_b \right], \quad (4.2)$$

$$E_{\text{pot}} = \frac{1}{2\rho} \sum_b (\Sigma_b^{0(0)} \rho_b - \Sigma_b^S \rho_b^S). \quad (4.3)$$

In Fig. 6 the results for the kinetic, potential, and total binding energy per particle in the DDRH model are given as functions of the density for temperatures from 0 to 30 MeV. Obviously, thermal excitations affect mostly the kinetic part of the energy, while the potential energy is nearly unaffected by temperature effects. The kinetic energy is also modified by many-body interactions through the inclusion of the self-consistent effective masses M_b^* . At $T = 0$ this can be seen by comparing the DDRH result and the corresponding result for a noninteracting gas. The latter is indicated by the dashed curve in Fig. 6. Because the effective mass is decreasing with density, nucleon-nucleon interactions result in a repulsive effect in the kinetic energy.

The repulsion of E_{kin} is partially compensated by the potential energy. E_{pot} is negative in the whole density range and decreases constantly with ρ . At lower temperatures the attraction of the potential energy is strong enough to create a binding in the total energy. The interplay between the repulsive and the attractive character of the two energies shows up as a local minimum in E_B , defining the saturation point ρ_0 of nuclear matter. In the DDRH calculation at $T = 0$ the

TABLE I. Comparison of the nuclear-matter equilibrium properties at $T = 0$.

Model	ρ_0 (fm $^{-3}$)	$E_B(\rho_0)$ (MeV)	K	M_b^*	E_{sym}
DDRH	0.181	-15.94	282	518	26.7
DD-ME2	0.153	-16.54	251	534	32.3
NL3 [25]	0.148	-16.3	272	562	37.4
SLy230a [27]	0.160	-16.0	230	655	32.0
QHD	0.192	-15.4	530	524	33.7

saturation point is found at $\rho_0 = 0.18$ with $E_B(\rho_0) = -15.94$, which is very close to DBHF calculations. A comparison of the equilibrium properties at $T = 0$ between the different models is given in Table I. With rising temperature the repulsion of E_{kin} becomes stronger, leading to a less bound system. For $T > 22$ MeV E_B stays positive in the whole density range. In the $\rho \rightarrow 0$ limit the kinetic energy, and thus E_B , comes very close to the classical value of an ideal gas, $E_B = 3/2T$.

The effect of density-dependent interactions on the EOS in the DDRH model can be better understood by examining the functional behavior of the rearrangement self-energy Σ^R . In Fig. 7 we show Σ^R as a function of the baryon density ρ for symmetric nuclear matter at fixed temperatures. Obviously, Σ^R is very small compared to the Hartree self-energies $\Sigma^{(0)}$ (≈ 350 MeV at saturation density ρ_0). This justifies the expansion of the Hamiltonian up to the first order in the density deviation as described in the previous section. The temperature dependence of Σ^R comes mainly from the scalar densities ρ_b^s , which saturate for $\rho \gg \rho_0$. Therefore, Σ^R becomes independent of temperature in the high-density limit. In the region of nuclear-matter saturation density, ρ_0 , the rearrangement contributions are more sensitive to temperature changes. However, the functional deviations are still rather small here and one can consider Σ^R as independent of temperature for $T < 20$ MeV.

The influence of the rearrangement energies on the pressure is illustrated in Fig. 8. The full DDRH calculation (solid lines) is compared to calculations without rearrangement terms (dashed lines). In contrast to the self-energies, the rearrangement contributions have a significant effect on the

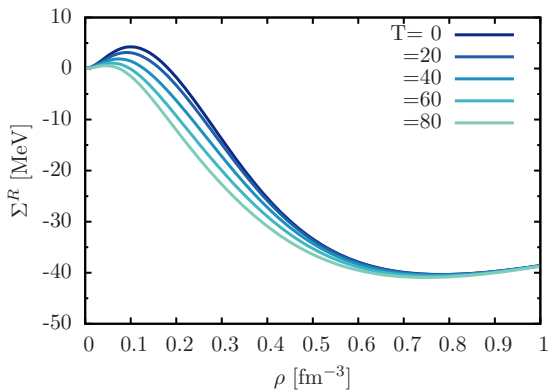


FIG. 7. (Color online) The rearrangement self-energy Σ^R as a function of baryon density ρ at various values of temperature T (in MeV). Lower curves correspond to higher temperatures.

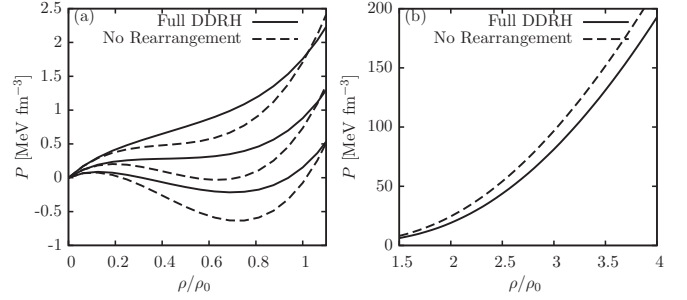


FIG. 8. The rearrangement contributions to the pressure. (a) Low-density region for $T = 10, 15$, and 20 MeV (lower curves correspond to lower T). (b) High-density region for $T = 20$ MeV.

nuclear-matter pressure. Their modification on P is even contrary in the low- and high-density regions. While for $\rho < \rho_0$ the rearrangement terms cause an increase in the pressure density, their inclusion softens P for $\rho > 1.5\rho_0$. This is, of course, a direct consequence of the functional dependence of Σ^R on ρ and T , because $P^R = \rho \Sigma^R$.

The increase of the pressure at low densities plays a crucial role on the liquid-gas phase transition region of nuclear matter.

Figure 9 shows the pressure $P(T, \rho)$ of symmetric nuclear matter as a function of the nucleon density ρ for fixed values of the temperature T (isotherms). The curves exhibit the characteristics of a typical first-order liquid-gas phase transition. In the low-temperature region the pressure first increases slightly with the density, then decreases to its minimum point and finally returns to a continuous rising in the high-density region, where it asymptotically approaches the causality limit $P = \mathcal{E}$ (Fig. 10). This functional behavior is very similar to the one of a classical van der Waals liquid [44].

Next we discuss the entropy in the DDRH approach. Entropy production plays an important role in the determination of the mass fragment distribution in multifragmentation events of heavy-ion collisions [45]. In Fig. 11 the density and temperature dependence of the entropy per particle, $S/A = S/\rho$, is shown. The left panel shows S/A as a function of density for fixed temperatures in the range of 0–30 MeV. First of all, we can see that the entropy increases with temperature

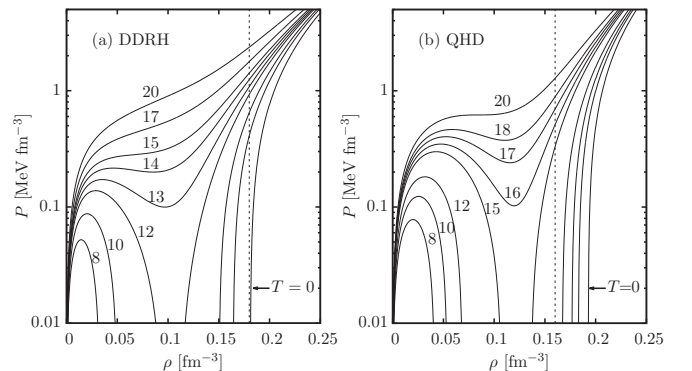


FIG. 9. Comparison of the EOS $P[\varepsilon(\rho)] = P(\rho)$ for symmetric nuclear matter at various temperatures. The numbers denote the temperature T in MeV.

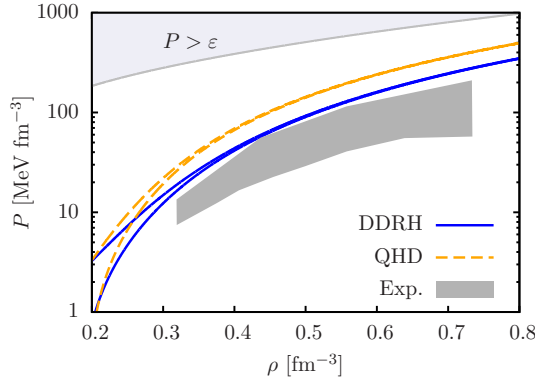


FIG. 10. (Color online) Functional behavior of the pressure P in the high-density region for symmetric nuclear matter. The graph shows the results at $T = 0$ MeV (lower curves) and $T = 20$ MeV (upper curves) for DDRH and QHD models. The gray region corresponds to the region of pressures consistent with the experimental flow data. The upper blue shaded area, labeled by $P > \epsilon$, exhibits the causality limit.

and significantly decreases with density. This behavior is what is expected given the fact that entropy is a measure of thermal disorder. At $\rho \rightarrow \infty$, S/ρ saturates at values in the range of 0.5–1.0 for the considered temperatures. Additionally, there are two notable limits. First, at low densities the entropy approaches the logarithmic density dependence of a classical system, $S/A \sim -\ln(\rho)$. This can be ascribed to the fact that in the regime of very low densities as well as high temperatures quantum effects become less important and thus the properties of a classical system are recovered. However, the temperature dependence of S/A approaches a linear behavior at $T \rightarrow 0$, as shown on the right panel of Fig. 11. This becomes even more pronounced at higher densities. In this regime, the system can be assumed as a Fermi liquid, where the relation between S is given by

$$\frac{S_{\text{FL}}}{A} = \frac{\pi^2}{2\rho} N_F T, \quad (4.4)$$

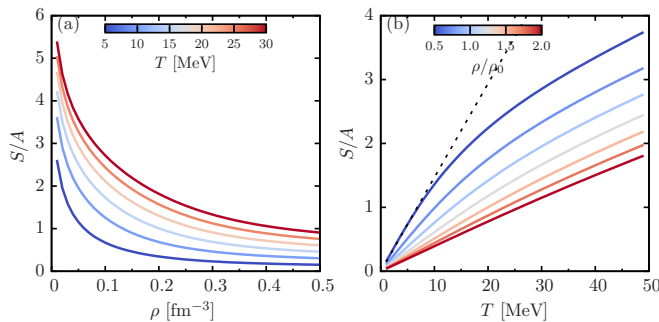


FIG. 11. (Color online) Entropy per particle. (Left) As a function of ρ for fixed T from 5 to 30 MeV in steps of 5 MeV. The dashed line shows the classical limit at $T = 30$ MeV. (Right) As a function of T for fixed density values from $0.5\rho_0$ to $2\rho_0$ in steps of $\frac{1}{4}\rho_0$. The dashed line shows the limit of a Fermi liquid as explained in the text.

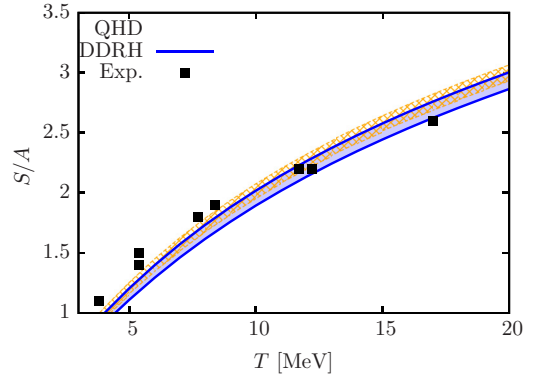


FIG. 12. (Color online) Comparing the entropy per particle from the DDRH calculations to experimental results [47]. The theoretical band corresponds to $0.047 \leq \rho \leq 0.053 \text{ fm}^{-3}$, accounting for the uncertainties in the experimental analysis.

where

$$N_F = \frac{E_F k_F}{\pi^2} \quad (4.5)$$

is the density of states at the Fermi surface [46].

In Fig. 12 we compare the DDRH calculation of S/A to results obtained from Au + Au collisions at energies between 100 and 400 A MeV [47]. The experimental data were obtained from the study of the fragments which remain after the collision. By assuming that the dense fireball created in the interior of a collision is in thermal equilibrium, information on the entropy per particle of the fireball can be obtained, in principle, from the fragmentation remnants of the collision; see, e.g., Ref. [15]. However, this analysis comes with some uncertainties owing to statistical assumptions that might not be fully satisfied in a heavy-ion collision. Apart from that, one assumes that the freeze-out density of the fireball is $\rho \approx 0.3\rho_0$. This provides a further uncertainty in the calculation. To account for small deviations from this central density, we show the theoretical results in the range of $0.047 \leq \rho \leq 0.053 \text{ fm}^{-3}$. Although we find that in this density and temperature range the differences between the DDRH and the simple QHD model are very small, the DDRH results indicate a slightly better agreement with the data for temperatures higher than 10 MeV. Nevertheless, one should note that a clear distinction between the models is barely possible for this set of data.

We conclude the set of results for symmetric nuclear matter with the discussion of the free energy per particle, $F/A = \mathcal{F}/\rho = (\mathcal{E} - TS)/\rho$. Figure 13 shows \mathcal{F}/ρ as a function of density and temperature. At very low temperatures the free energy has a local minimum, which is the equivalent to the saturation point of nuclear matter at $T = 0$. At finite temperatures the equilibrium state of the system is given by the minimization of the free energy instead of the energy density. This minimum describes a thermodynamically preferred state of the system. The local minimum of the free energy disappears above the so called flashing temperature, T_F . At this point the pressure is still high enough to prevent the system from decaying to the low-density (gas) phase, leading to a liquid-gas coexistence. Above a critical temperature, T_C , this coexistence

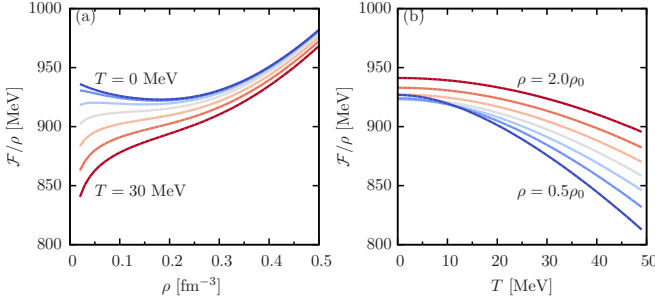


FIG. 13. (Color online) The free energy per particle. Isotherms are chosen the same as in Fig. 11.

does not hold any longer and the system is found in the thermodynamically preferred state at very low densities. For the DDRH model we find the following values for the flashing and critical temperatures of symmetric nuclear matter:

$$T_F^{\text{DDRH}} \approx 12.2, \quad T_C^{\text{DDRH}} \approx 14.6.$$

Although E/A is more repulsive with rising temperature, the free energy per particle is a decreasing function of T . Obviously, this behavior can be ascribed to the $-TS$ term and thus is a pure entropic effect. The same applies to the $\rho \rightarrow 0$ limit, where classical effects dominate the properties of the system (compare Fig. 11) [48].

The analysis of symmetric nuclear matter shows that nucleon-nucleon interactions affect the bulk properties of nuclear matter in two ways. First, they obviously give rise to the potential energy. Second, the interactions invoke self-consistent effective masses and chemical potentials. Especially the latter quantities affect both the thermal and the spectral distribution functions of the nucleons. Therefore, the in-medium interactions have a remarkable effect on the kinetic part of the (free) energy, effectively increasing the kinetic energy.

In the considered density and temperature range, our results for the DDRH model are in good agreement with experimental data, as well as other microscopic DBHF calculations [41]. This shows that the approximations applied here to the density-dependent vertices are not only suitable for the description of nuclear matter in the vicinity of the saturation point at $T = 0$, but lead also to reliable results in higher density as well as temperature regions.

V. ISOSPIN-ASYMMETRIC NUCLEAR MATTER

A. Thermal properties of asymmetric nuclear matter

In the previous section we studied the results for nuclear matter with equal content of protons and neutrons. In this section we study isospin effects in warm nuclear matter at moderate temperature well below the critical temperature T_C of the QCD phase transition. For this purpose, we introduce the proton fraction $\xi \equiv \rho_p/\rho$ as an indicator for charge asymmetry and the isospin content. In the DDRH model, the inclusion of the scalar isovector δ meson field leads to a separation of the proton and neutron effective masses in asymmetric nuclear matter. In Fig. 14 we plot the ratio between the effective and the

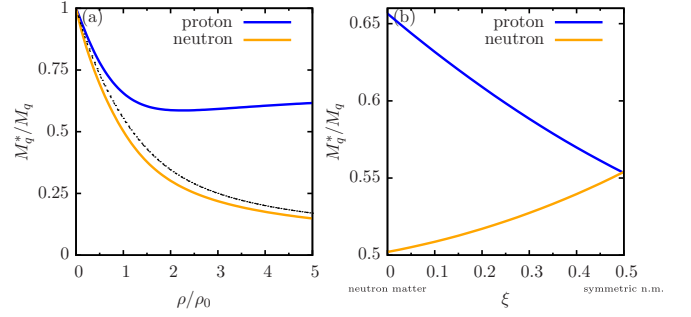


FIG. 14. (Color online) Effective nucleon masses M_q^* ($q = p, n$) for protons (upper blue line) and neutrons (lower orange line) at $T = 0$ as functions of the total baryon density for pure neutron matter (left) and as functions of the asymmetry parameter $\xi = \frac{Z}{A}$ at saturation density $\rho = \rho_0$ (right). The thin dashed curve in the left panel represents the result in case of symmetric nuclear matter.

corresponding bare nucleon masses. The black dashed curve on the left panel shows the result for symmetric nuclear matter ($\xi = 0.5$). In this case, $M_p^* = M_n^*$ decreases continuously with ρ . As the asymmetry increases (i.e., smaller values of ξ), protons gain a larger effective mass, while the effective mass of neutrons decreases. It is particularly interesting to note that the isospin effect on M_p^* is much stronger than on M_n^* . In the limit of $\xi = 0$ (neutron matter), M_n^* deviates only slightly from its symmetric nuclear-matter value, whereas M_p^* shows a considerable increase and even exhibits a local minimum at $\rho \approx 2.3\rho_0$. This behavior is a direct consequence of the self-consistent solution of the effective masses and scalar densities.

Figure 15 shows the energy density and pressure at $T = 0$ for values of ξ from pure neutron matter ($\xi = 0$) to symmetric nuclear matter ($\xi = 0.5$). As seen, the local minimum of the binding energy per particle shifts to the left, i.e., to lower densities, while the binding of the system reduces with increasing neutron excess. For $\xi < 0.05$ neutron-rich matter is completely unbound. At this point the potential energy is not strong enough to compensate the kinetic energy of the system. Hence, both energy density and pressure increase with decreasing proton fraction. In neutron-rich matter, the local minimum of the pressure disappears as well, as the right panel of Fig. 15 shows.

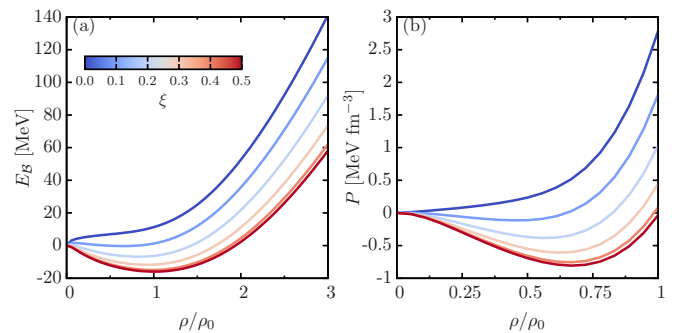


FIG. 15. (Color online) The binding energy (left) and the pressure (right) at $T = 0$ for values of ξ from 0 to 0.5 in steps of 0.1. Lower curves belong to lower values of ξ .

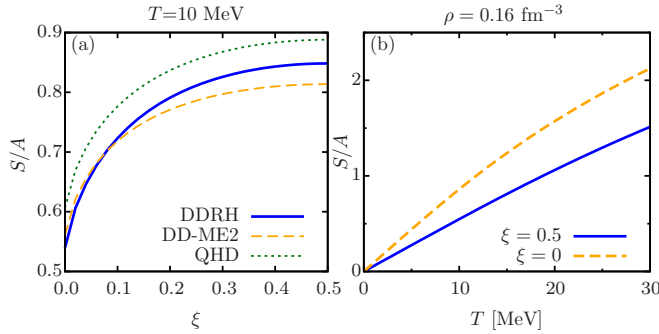


FIG. 16. (Color online) (Left) The entropy per particle as a function of the proton fraction ξ at $T = 10$ and $\rho = 0.16 \text{ fm}^{-3}$. The results for the DDRH, DD-ME2 [24], and QHD parametrization are shown. (Right) Comparison of the temperature dependence of the entropy per particle between symmetric (upper curve) and pure neutron matter (lower curve) in the DDRH model at fixed density $\rho = 0.16 \text{ fm}^{-3}$.

Thus, the thermodynamically preferred state of neutron matter is a dilute Fermi gas in the entire density range.

The entropy S/A decreases for smaller values of ξ as the degrees of freedom are reduced in systems with smaller proton fractions. In our calculations, we find a very similar asymmetry dependence of S/A in the whole temperature range. As an example, we show S/A as a function of ξ within several models at a fixed temperature of $T = 10$ MeV. The results show that the calculation with the linear QHD parametrization produces somewhat larger values of the entropy. The blue solid curve of the DDRH calculation lies above the results with the phenomenological DD-ME2 parametrization [24]. This difference is less pronounced at smaller ξ , however, and at neutron matter the entropy in the DDRH model is even slightly smaller than the one of the DD-ME2 calculation. In the right panel of Fig. 16 we compare the entropy per particle as a function of the temperature between symmetric nuclear matter and neutron matter within the DDRH model. For neutron matter S/A shows a linear temperature dependence throughout almost the whole temperature range.

In Fig. 17 the free energy per particle of neutron matter is compared between the DDRH and the phenomenological DD-ME2 model. The results show that the DDRH parametrization leads to a less repulsive free energy, which is a consequence of the additional attraction in the scalar-isovector channel. At low densities the curves of the two models coincide with each other, because the differences between the interactions become less important in this density region. As in the case of symmetric nuclear matter, F/A decreases with temperature owing to the higher values of the entropy.

To investigate the isospin-dependent part of the EOS, consider the expansion of the free energy in powers of the isospin parameter $\alpha \equiv (\rho_n - \rho_p)/\rho$ around symmetric nuclear matter ($\alpha = 0$):

$$F(\alpha, \rho, T) = F(0, \rho, T) + F_{\text{sym}}(0, \rho, T)\alpha^2 + \mathcal{O}(\alpha^4). \quad (5.1)$$

Because of isospin symmetry, odd powers of α vanish in the above expansion. Equation (5.1) defines the free symmetry energy, F_{sym} , which is related to the cost of converting

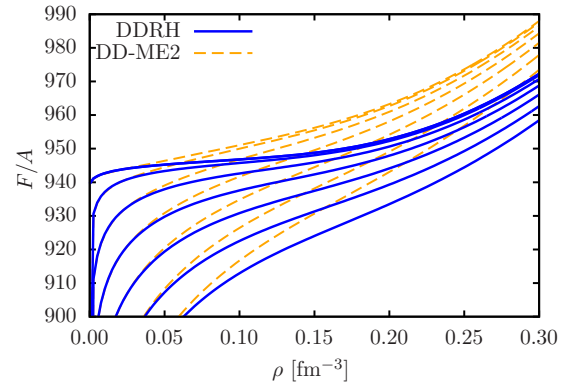


FIG. 17. (Color online) Free energy per particle in neutron matter for temperatures from 0 to 30 MeV in equidistant steps of 5 MeV (lower curves correspond to higher temperatures). The results of the DDRH (solid lines) and the DD-ME2 (dashed lines) model are compared.

protons into neutrons in the nuclear medium. Accordingly, the symmetry energy, E_{sym} , and the symmetry entropy, S_{sym} , can be defined in the same way. The relation to the proton fraction parameter ξ is then given by

$$A_{\text{sym}} = \frac{1}{8} \frac{1}{\rho} \frac{\partial^2 \mathcal{A}}{\partial \xi^2} \Big|_{\xi=0.5}, \quad \mathcal{A} \in \{\mathcal{F}, \mathcal{E}, \mathcal{S}\}. \quad (5.2)$$

As usual, the above symmetry functionals follow the general thermodynamic relation $F_{\text{sym}} = E_{\text{sym}} - T S_{\text{sym}}$.

The symmetry energy plays a fundamental role in the description of many important phenomena in nuclear physics, such as the structure of exotic nuclei, heavy-ion collisions, and neutron stars. In the past decade the density dependence of the symmetry energy has been extensively studied both experimentally and theoretically [49]. In addition, the knowledge of the temperature dependence of the (free) symmetry energy has become more and more important in connection with the analysis of multifragmentation data of hot nuclear matter. It is also an important ingredient in astrophysical calculations such as the evolution of protoneutron stars or the core collapse of a massive star and the associated explosive nucleosynthesis [50,51]. In the last years some progress has been achieved in heavy-ion collision experiments to extract the temperature dependence of F_{sym} at low densities [52].

In Fig. 18 we show our prediction for F_{sym} and E_{sym} (see also Table II). Again, results for DDRH and DD-ME2 parameter sets are compared together with the experimental data points from charge exchange reactions [53], neutron skin analysis [54], and heavy-ion collisions [55]. The symmetry energy of the DDRH model shows a stiff density dependence, while it is soft for the phenomenological DD-ME2 model parameter set. At $T = 0$ and at low densities both models describe the experimental data quite well. At saturation density the DDRH parametrization slightly underestimates the experimental value for E_{sym} . However, because—contrary to the DD-ME2 model—the DDRH parameter set has not been fitted to experimental data, this result is already quite noteworthy. As for the temperature dependence, one can

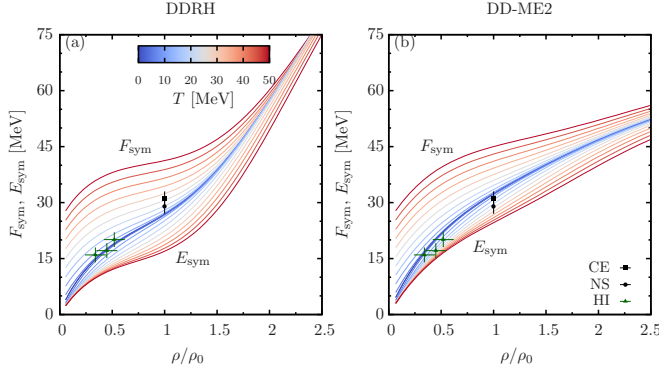


FIG. 18. (Color online) Symmetry and free symmetry energy as functions of the density for fixed values of T from 0 to 50 MeV. At $T = 0$ (blue curve) $F_{\text{sym}} = E_{\text{sym}}$. Curves above (below) the zero temperature line correspond to F_{sym} (E_{sym}). The right and the left panels show the results for the DDRH and DD-ME2 models, respectively. The points indicate experimental results for the symmetry energy at $T = 0$. The data points are taken from [53] (CE), [54] (NS), and [55] (HI).

see that F_{sym} and E_{sym} show an opposite behavior. While F_{sym} increases with T , E_{sym} becomes smaller with rising temperature. The decrease of E_{sym} at higher temperatures can be understood from the fact that the Fermi surface is more diffuse and therefore the Pauli blocking becomes less important at increasingly higher temperatures. The increase of the free symmetry energy, however, is related to the negative value of S_{sym} , because the total entropy per particle decreases with increasing asymmetry (Fig. 16). Consequently, F_{sym} is expected to be larger than E_{sym} at fixed density and temperature values. Additionally, the entropic effect of the free symmetry energy is stronger than the decrease of E_{sym} , which, all in all, causes F_{sym} to increase with T .

B. Phase transitions in asymmetric nuclear matter

As a starting point, let us first recall some basic concepts of phase transitions in nuclear matter. The EOS of nuclear matter shows a typical van der Waals gas behavior at temperatures $0 < T < 20$ MeV [44] (see Fig. 9). Below a critical temperature T_C one finds a region where $\frac{\partial P}{\partial \rho}|_T < 0$. This is the region of mechanical instability where the preferred state of the system is given by two coexisting phases. The thermodynamical equilibrium of the two phases can be obtained with the help of

TABLE II. E_{sym} and F_{sym} taken at saturation density for different values of temperature T in the DDRH and DD-ME2 models.

T (MeV)	$E_{\text{sym}}^{\text{DDRH}}$ (MeV)	$E_{\text{sym}}^{\text{DD-ME2}}$ (MeV)	$F_{\text{sym}}^{\text{DDRH}}$ (MeV)	$F_{\text{sym}}^{\text{DD-ME2}}$ (MeV)
10	26	32	27	33
20	24	30	29	35
30	21	28	32	37
40	19	26	36	41
50	17	25	41	45

the Gibbs-Duhem relation,

$$dP - SdT - \sum_c \rho_c d\mu_c = 0, \quad (5.3)$$

where the sum includes all conserved charges. Equation (5.3) applies to both phases separately. In case of one conserved charge, this leads to the Gibbs conditions

$$\mu^{\text{I}}(\rho^{\text{I}}, T) = \mu^{\text{II}}(\rho^{\text{II}}, T), \quad (5.4)$$

$$P^{\text{I}}(\rho^{\text{I}}, T) = P^{\text{II}}(\rho^{\text{II}}, T), \quad (5.5)$$

where the labels I and II refer to the two phase states, with the convention $\rho^{\text{I}} < \rho^{\text{II}}$. Recalling that the preferred state of a system is the one with the lowest value of the free energy, we can write the global stability condition for the mixed phase [9],

$$\mathcal{F}(\rho, T) < \lambda \mathcal{F}(\rho^{\text{I}}, T) + (1 - \lambda) \mathcal{F}(\rho^{\text{II}}, T), \quad (5.6)$$

with

$$\rho = \lambda \rho^{\text{I}} + (1 - \lambda) \rho^{\text{II}} \quad \lambda \in [0, 1],$$

where the parameter λ determines the volume fraction occupied by each phase. Equation (5.6) implies that for a stable system \mathcal{F} should be a convex function of the density,

$$\frac{\partial^2 \mathcal{F}}{\partial \rho^2} \geq 0.$$

Note that the above expression is equivalent to $\frac{\partial \mu}{\partial \rho} \geq 0$, as can be easily deduced from $d\mathcal{F} = -SdT + \sum_c \mu_c d\rho_c$. With this, the phase transition region is characterized by the following states:

- (i) *spinodal curve*, describes the onset of the instability region, $\frac{\partial^2 \mathcal{F}}{\partial \rho^2} = 0$;
- (ii) *metastable region*, the stability conditions are fulfilled locally, but Eq. (5.6) is violated;
- (iii) *binodal curve*, describes the onset of the metastable states.

Hence, the two-phase coexistence area is enclosed by the binodal curve. Within this area the pressure and the chemical potentials are kept constant. The projection of the coexistence area onto the T - P or T - μ plane results in the first-order phase transition lines. Together with the T - ρ phase diagram they provide a full description of the phase transition. In Fig. 19 we present the DDRH results of the T - ρ (left) and the T - P (right) phase diagrams. The hatched area indicates the region of mechanical instability. We find a critical temperature of $T_C \approx 14.55$ MeV. The calculation with the DD-ME2 parameter set provides similar results, although the values of the critical points are a bit smaller than in the DDRH case.

The above conditions can be generalized to describe phase transitions of multicomponent systems with N conserved charges, e.g., hypernuclear matter. The stability criterion (5.6) then holds for each conserved charge density ρ_i . The resulting set of N inequalities implies [9]

$$\frac{\partial \mu_i}{\partial \rho_j} = \frac{\partial \mu_j}{\partial \rho_i} > 0. \quad (5.7)$$

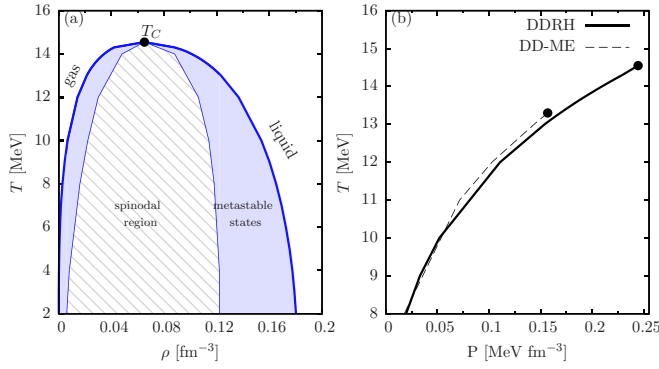


FIG. 19. (Color online) The phase transition diagrams of symmetric nuclear matter. (Left) The T - ρ phase diagram in the DDRH model. The binodal and spinodal curves are indicated by thick and thin lines, respectively. (Right) The T - P phase diagram for the DDRH and DD-ME2 model calculations.

In the coexistence region the Gibbs conditions of a multicomponent system have to be fulfilled for each particle type,

$$\mu_i(\rho_i^I) = \mu_i(\rho_i^{II}), \quad P(\rho_i^I) = P(\rho_i^{II}). \quad (5.8)$$

For isospin-asymmetric nuclear matter the conserved charges of the system are given by the baryon number B and the third component of the total isospin I_3 . Any state of the nuclear-matter system can thus be characterized by the baryon density $\rho_B = \rho_p + \rho_n$ and the isovector density $\rho_3 = \rho_p - \rho_n$. The corresponding baryon and isospin chemical potentials are related to the nucleon and proton chemical potentials through

$$\mu_B = \mu_p + \mu_n, \quad \mu_3 = \mu_p - \mu_n.$$

It is feasible to express the stability conditions in terms of the proton fraction ξ ,

$$\rho \left(\frac{\partial P}{\partial \rho} \right)_{T,\xi} > 0, \quad \left(\frac{\partial \mu_p}{\partial \xi} \right)_{T,P} > 0, \quad \left(\frac{\partial \mu_n}{\partial \xi} \right)_{T,P} < 0. \quad (5.9)$$

The last two expressions are referred to as *chemical stability conditions*. They take into account the fact that there is energy needed to change the concentration of protons in the medium at a fixed temperature and pressure. The chemical instability region is found from the analysis of the neutron and proton chemical potential isobars as functions of ξ . In Fig. 20 a set of isobars in the range of $0.1 \text{ MeV fm}^{-3} < P < 0.25 \text{ MeV fm}^{-3}$ is shown. One can see an area in the P - ξ space, where the chemical stability conditions are violated. In this section the system would break apart into two phases with different concentrations of its constituents. With increasing pressure the instability region becomes smaller until it disappears completely at the critical pressure P_C . At this point an inflection point appears in the chemical potential isobars,

$$\left(\frac{\partial \mu}{\partial \xi} \right)_{T,P=P_C} = \left(\frac{\partial^2 \mu}{\partial \xi^2} \right)_{T,P=P_C} = 0.$$

In models with constant nucleon-meson couplings the position of the inflection points of protons and neutrons coincides in

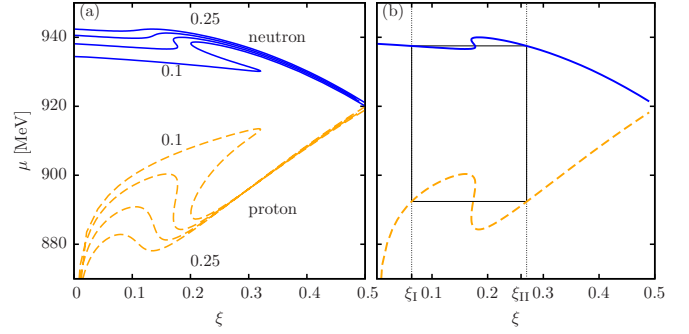


FIG. 20. (Color online) The chemical potential isobars of nuclear matter in the DDRH model as a function of ξ at $T = 10 \text{ MeV}$. The left panel shows the neutron (solid blue line) and proton (dashed orange line) isobars for values of P from 0.1 to 0.25 MeV fm^{-3} . The right panel indicates the geometrical construction in case of $P = 0.15 \text{ MeV fm}^{-3}$ as described in the text.

the P - ξ plane. This assumption is, however, no longer true once the couplings become density dependent. In this case, the chemical potential of one type of nucleons can pass an inflection point while the other one still has an unstable region. This circumstance was first found by Qian [56], where it was shown that the asynchronous behavior of the nucleon species varies according to the density dependence of the isovector-vector coupling, Γ_ρ . In agreement with that, we find a similar situation for the DDRH model.

In phase equilibrium, the pressure and the chemical potentials of the two phases are equal, as required by the Gibbs conditions. The two solutions to this requirement can be found by means of a geometrical construction, as shown in the right panel of Fig. 20 [57]. The points ξ_I and ξ_{II} indicate the onset of the coexistence region. Thus, owing to the additional degree of freedom, the binodal curve becomes a surface in the T - P - ξ space. To better visualize this surface, it is usually displayed in slices at constant T , which is referred to as the *binodal section*. The shape of the binodal section depends highly on the model of the nucleon-nucleon interaction.

To illustrate the nature of the liquid-gas transition in asymmetric nuclear matter, we show the result of the binodal section of the DDRH model at $T = 10 \text{ MeV}$ in Fig. 21. Following the notation of Ref. [9], we indicate some characteristic points of the curve. By MA the point at maximum asymmetry is indicated. For $\xi < \xi_{MA}$ the system stays in the gas phase and a phase transition does not take place. The point of equal concentration, EC, lies at $\xi = 0.5$, reflecting the one-component character of symmetric nuclear matter. The critical point CP (ξ_C, P_C) indicates the edge of the instability area. For $P > P_C$ the chemical potentials of protons and neutrons are monotonically with ξ .

In the phase coexistence region the system favors a configuration with different proton concentrations of the two phases. This does not violate the isospin conservation law, because only the sum of the isospin of the two phases needs to be conserved. One finds that the phase with lower ξ (higher asymmetry) takes the lower density. The points CP and EC divide the binodal section into two branches, where the left (right) branch corresponds to the phase with lower (higher)

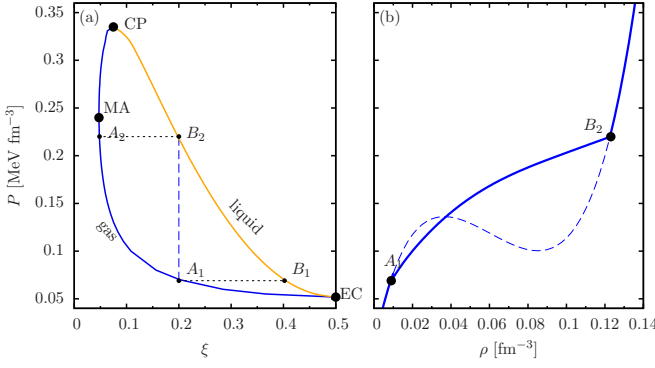


FIG. 21. (Color online) The binodal section at $T = 10$ MeV in the DDRH model. The right panel shows the projection of the points A_1 and A_2 on the pressure at fixed proton concentration $\xi = 0.2$.

density and proton concentration. Thus, the left branch is associated with the gas phase and the right one with the liquid phase. The binodal section shrinks with temperature, i.e., P_{CP} becomes smaller and MA shifts to higher values of ξ . At $T = T_C$ the points CP, MA, and EC coincide at $\xi = \frac{1}{2}$ and the binodal surface finally reduces to a single point.

In contrast to symmetric nuclear matter, the pressure does not stay constant during a phase transition. This arises from the fact that the two phases follow the two different branches along the binodal curve. As an example, consider a system in a configuration below the binodal section with $\xi = 0.2$. As the system is isothermally compressed, it will reach the two-phase instability region at the point A_1 . In this stage a second phase emerges at the point B_2 with $\xi \approx 0.4$ (liquid phase). During the phase transition the total proton fraction ξ is held fixed, as indicated by the vertical line in the left panel of Fig. 21. The two coexisting phases evolve along the two different branches of the binodal section. The gas phase follows the left branch from A_1 to A_2 and the liquid phase follows the right branch from B_1 to B_2 . Finally, the system leaves the instability area at the point B_2 . The solution of the equations

$$\begin{aligned}\rho &= \lambda \rho^I + (1 - \lambda) \rho^{II}, \\ \rho_3 &= (2\xi - 1)\rho = \lambda \rho_3^I + (1 - \lambda) \rho_3^{II},\end{aligned}$$

provides the fraction λ of the volume which is occupied by the gas phase. In the above example, $\lambda = 1$ at A_1 and vanishes at A_2 , implying that the system evolves from a gas to a liquid phase. The solution of the above equations can be used to calculate the behavior of the pressure during the phase transition. This is illustrated in the right panel of Fig. 21.

The behavior of the system during an isothermal compression can be very different depending on the asymmetry parameter. In general, one can distinguish between the following two condensation types.

- (i) $\xi > \xi_s$: *Stable condensation*. Starting in the gas phase, the system undergoes a phase transition and ends in the stable liquid phase.
- (ii) $\xi < \xi_s$: *Retrograde condensation*. The system starts and terminates its evolution through the two-phase coexistence region in the gas phase. The liquid phase that emerges during the transition disappears again as

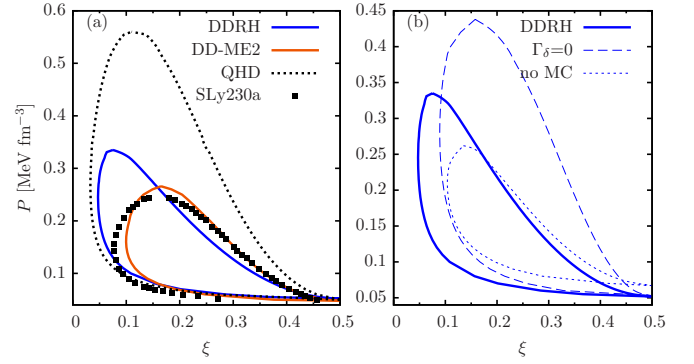


FIG. 22. (Color online) (a) Comparison of the binodal surface at $T = 10$ MeV among the DDRH, DD-ME2, QHD, and SLy230a [10] models. (b) Results of calculations without δ meson interaction (dashed line) and without momentum correction (short dashed line) are compared to the full DDRH calculation.

the upper boundary of the binodal section is reached. This behavior does not occur in a one-component system.

It is interesting to examine how the shape of the binodal section depends on the nucleon-nucleon interaction. Especially the position of the characteristic points is very sensitive to the isospin part of the interaction. In Fig. 22(a) the binodal section at $T = 10$ MeV of the DDRH model is compared to the results from other models. A summary of the corresponding critical values can be found in Table III.

As in the case of symmetric nuclear matter, density-dependent interactions provide a much smaller coexistence region. In the QHD model the instability region extends to $P \approx 0.56$ MeV fm $^{-3}$. The DDRH binodal stretches to much smaller values of the asymmetry parameter ξ than the one of the phenomenological DD-ME2 model. The point of maximum asymmetry is found at $\xi_{MA} \approx 0.05$ and $\xi_{MA} \approx 0.1$ in the DDRH and DD-ME2 cases, respectively. We also display the result of the nonrelativistic Skyrme-type interaction SLy230a

TABLE III. Comparison of the critical point parameters for several temperatures. The results for the NL3 and SLy230a models are taken from Ref. [10].

	T (MeV)	ξ_c	ρ_c (fm $^{-3}$)
DDRH	0	0.0135	0.059
DD-ME2	0	0.0025	0.0327
NL3	0	0.0567	0.0766
SLy230a	0	0.0149	0.0843
DDRH	10	0.077	0.079
DD-ME2	10	0.167	0.065
NL3	10	0.1785	0.0573
SLy230a	10	0.110	0.0608
DDRH	14.55	0.5	0.0653
DD-ME2	13.31	0.5	0.045
NL3	14.55	0.5	0.0463
SLy230a	16.52	0.5	0.0535

by Dutra *et al.* [10]. The DD-ME2 binodal is remarkably close to the one of the SLy230a model. This circumstance can be related to the way the isovector channel is parametrized in the corresponding models, as was also found by Dutra *et al.* To illustrate this more clearly, we show in Fig. 22(b) the impacts of the isovector-scalar δ channel and the momentum correction in the DDRH model on the binodal shape. The dashed curve represents the result without the δ meson interaction, where $\Gamma_\delta = 0$. One can see that the δ interaction increases the value of the maximum asymmetry. The short dashed line represents the solution without momentum corrections where we set all momentum correction parameters (C_S) to zero. One can see that momentum correction leads to lower values of ξ_{MA} by approximately the same extent as of the δ interaction. It is also interesting to note that the binodal sections of the DD-ME2 and SLy230a models are very close to the one of the DDRH model without momentum correction terms.

In conclusion to this discussion, we study the asymmetry dependence of the critical temperature. First of all, we should remark that in the case of asymmetric nuclear matter the definition of the critical temperature is used differently in the literature [58]. Some authors define the critical temperature for a given value of ξ such that ξ corresponds to ξ_C at $T = T_C$. In this way the system remains in the gas phase for $T > T_C$ [59]. However, many authors prefer the definition which is equivalent to the one of symmetric nuclear matter, that is, where the pressure has an inflection point in the P - ρ phase diagram. This definition represents the temperature from which the system remains mechanically stable, although a chemical instability may still be present at this point. Therefore, one should rather refer to this temperature as the critical temperature of mechanical instability, T_{CM} . Because the calculation of T_{CM} is more straightforward and also more familiar, it is widely used in the literature [48,60,61]. T_{CM} is somewhat smaller than T_C , yet it also represents the asymmetry dependence of the instability region.

In Fig. 23 we show the mechanical critical temperature as a function of ξ for different models. T_{CM} decreases continuously

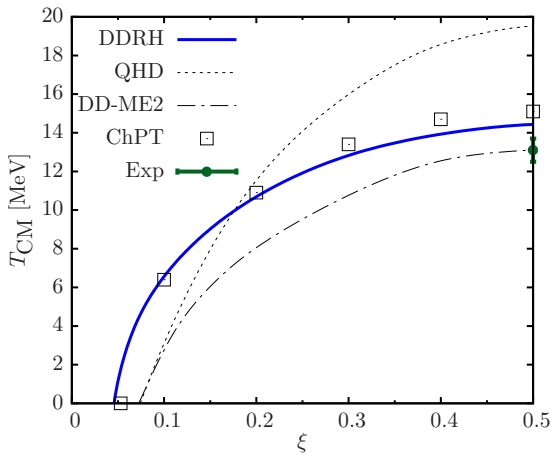


FIG. 23. (Color online) The critical temperature of mechanical instability as a function of the proton fraction ξ . The results are compared between different models. The good agreement between our DDRH and the ChPT results of Ref. [48] is remarkable.

TABLE IV. Comparison of the critical temperatures, T_{CM} (MeV), at different asymmetry values ξ .

ξ	DDRH	DD-ME2	ChPT
0.5	14.6	13.3	15.1
0.4	14.0	12.6	14.7
0.3	12.8	10.8	13.4
0.2	10.7	8.1	10.8
0.1	6.6	2.6	6.5

with rising neutron excess and vanishes at $\xi = \xi_{CM}$. For asymmetry fractions below this value, the system remains mechanically stable at all temperatures. At higher values of ξ the curve of the QHD model lies above the curves of the other models, overshooting the experimental value of symmetric nuclear matter. Nevertheless, the curve falls off much faster with decreasing ξ and coincides with the DD-ME2 line at $T_{CM} = 0$. For comparison, recent results from chiral perturbation theory (ChPT) by Fiorilla *et al.* [48] also are displayed. In this calculation the one- and two-pion exchange diagrams as well as Δ -isobar degrees of freedom are explicitly taken into account. In Table IV we provide a summary of the results for some fixed values of the proton-neutron asymmetry ξ . It is remarkable that the DDRH result is very close to the one of ChPT throughout the whole ξ range. This indicates that in the DDRH the higher-order correlation effects on the isospin degree of freedom are implicitly included in the density-dependent terms of the isovector-vector and isovector-scalar channels.

VI. SUMMARY AND OUTLOOK

The EOS of asymmetric nuclear matter was studied in the microscopic DDRH approach. The approach, being based on a DB approach to in-medium interactions, incorporates the essential aspects of an *ab initio* description by relying only on a free-space NN interaction but deriving the medium-dependent modifications in a self-consistent manner. An important step is the projection of the medium dependence onto effective density-dependent meson-baryon interactions leading to the formulation of relativistic nuclear-field theory with vertex functionals depending on the field operators. As discussed above, in MFA the field theoretical functionals become functions of the nuclear density. The mean-field limit is treated as the leading-order term in an expansion around the ground-state expectation value of a given configuration of symmetric or asymmetric nuclear matter. While in former DDRH-related work investigations of cold nuclear and hypernuclear matter and applications to neutron stars and finite nuclei and hypernuclei were considered, in this paper we have applied the approach for the first time to nuclear matter at finite temperature $T > 0$. The nuclear EOS was investigated in RMF approximation for proton ratios $\xi = Z/A$ ranging from symmetric nuclear matter ($\xi = \frac{1}{2}$) to pure neutron matter ($\xi = 0$).

As a generic feature of the DDRH theory we have included for the first time also isovector-scalar fields, realized in nature by the $a_0(980)$ meson. Already by general symmetry

arguments this interaction channel must be included into the theory. The most important effect is that in asymmetric nuclear-matter protons and neutrons obtain different relativistic effective masses. Hence, the two species of nucleons become mechanically distinguishable, affecting directly the thermodynamical properties. Of particular importance is the quite different behavior of asymmetric matter at the phase boundaries.

Although there exist quite a number of studies on the thermodynamics of symmetric nuclear matter and pure neutron matter, much less attention has been paid on the properties of warm asymmetric nuclear matter. While symmetric nuclear matter can still be considered as a single-component Fermi gas, this is no longer possible in asymmetric nuclear matter. Unequal proton and neutron numbers are translating into differences in Fermi momenta and chemical potentials, thus changing the chemical composition and kinetic and, owing to isovector interactions, the mechanical properties of the protons and neutrons, hence making the two species thermodynamical distinguishable. Thus, as discussed in the previous sections, a much more involved theoretical treatment in terms of a two-component Fermi gas is required. The increased theoretical effort, however, is awarded by a much richer phase structure of asymmetric nuclear matter. As discussed in detail in Sec. III the phase structure of asymmetric nuclear matter is conveniently studied in terms of the total, isoscalar, and the isovector baryon chemical potentials, respectively, accounting for the conserved charges of the system, namely the total baryon number B and the third component $I_3 \sim \frac{\rho_n - \rho_p}{\rho}$ of the total isospin, which is synonym to the conservation of the total charge of the system. Against naive first expectations, it is not the number of protons and neutrons separately that is conserved, but the overall Noether charges are the conserved quantities. This is seen clearly at the phase transition boundaries: During the phase transition the baryonic composition might change as long as B and I_3 are conserved. As pointed out, the

density dependence and isospin structure of the in-medium interactions plays a crucial role for the thermodynamics of warm asymmetric nuclear matter, affecting directly the details of the phase structure of the system. These aspects were studied in due detail by comparing our fully microscopic DDRH results with results obtained with the purely phenomenological RMF approaches like the original scalar-vector model of Serot and Walecka and the density-dependent extensions as the DD-ME2-approach of Ring *et al.* Qualitatively, the three approaches lead to similar predictions on the thermodynamics of warm nuclear matter, but in detail the differences in nuclear dynamics are reflected by variations in the phase diagrams. The positive message of that comparison is that models describing cold nuclear matter properly are also close in their predictions for warm nuclear matter, at least in the temperature range below $t \sim 100$ MeV and a compression factor of up to two or three times nuclear saturation density. This result is certainly of interest for heavy-ion physics because it confirms and gives further confidence to the widely used treatment of heavy-ion collisions in terms of a transport theoretical description based on RMF-type dynamics.

Clearly, the approach presented here is open to further extensions. The inclusion of hyperons is one of the interesting cases, making it possible to study warm hypermatter. Adding in addition β equilibrium one will be able to describe warm neutron star matter, thus giving access to a more extended, new approach to the early stages of a neutron star just after the formation of a protonneutron star and the subsequent cooling phase.

ACKNOWLEDGMENTS

This work was supported in part by DFG Graduiertenkolleg Giessen-Kopenhagen-Helsinki *Complex Systems of Hadrons and Nuclei*, GSI Darmstadt, and Helmholtz Graduate School for Hadron and Ion Research.

-
- [1] G. Sauer, H. Chandra, and U. Mosel, *Nucl. Phys. A* **264**, 221 (1976).
 - [2] B. Friedman and V. R. Pandharipande, *Nucl. Phys. A* **361**, 502 (1981).
 - [3] M. Baldo and L. S. Ferreira, *Phys. Rev. C* **59**, 682 (1999).
 - [4] H. A. Weldon, *Phys. Rev. D* **26**, 1394 (1982).
 - [5] R. J. Furnstahl and B. D. Serot, *Phys. Rev. C* **41**, 262 (1990).
 - [6] W. Botermans and R. Malfliet, *Phys. Rep.* **198**, 115 (1990).
 - [7] B. ter Haar and R. Malfliet, *Phys. Rev. Lett.* **56**, 1237 (1986).
 - [8] B. ter Haar and R. Malfliet, *Phys. Rev. Lett.* **59**, 1652 (1987).
 - [9] H. Müller and B. D. Serot, *Phys. Rev. C* **52**, 2072 (1995).
 - [10] M. Dutra, O. Lourenço, A. Delfino, J. S. Sá Martins, C. Providência, S. S. Avancini, and D. P. Menezes, *Phys. Rev. C* **77**, 035201 (2008).
 - [11] S. L. Shapiro and S. A. Teukolsky, *Black Holes, White Dwarfs, and Neutron Stars* (Wiley-VCH Verlag, Weinheim, Germany, 1983).
 - [12] P. Gögelein, E. N. E. van Dalen, C. Fuchs, and H. Mütter, *Phys. Rev. C* **77**, 025802 (2008).
 - [13] T. Gaitanos, H. Lenske, and U. Mosel, *Progress in Particle and Nuclear Physics* **62**, 439 (2009)..
 - [14] T. Gaitanos, A. Larionov, H. Lenske, and U. Mosel, *Nucl. Phys. A* **881**, 240 (2012).
 - [15] J. Bondorf, A. Botvina, A. Ilinov, I. Mishustin, and K. Sneppen, *Phys. Rep.* **257**, 133 (1995).
 - [16] H. Lenske and C. Fuchs, *Phys. Lett. B* **345**, 355 (1995).
 - [17] C. Fuchs, H. Lenske, and H. H. Wolter, *Phys. Rev. C* **52**, 3043 (1995).
 - [18] F. Hofmann, C. M. Keil, and H. Lenske, *Phys. Rev. C* **64**, 034314 (2001).
 - [19] F. de Jong and H. Lenske, *Phys. Rev. C* **58**, 890 (1998).
 - [20] H. Lenske, in *Extended Density Functionals in Nuclear Structure Physics*, Lecture Notes in Physics, edited by G. A. Lalazissis, P. Ring, and D. Vretenar, Vol. 641 (Springer, Berlin, Heidelberg, 2004), pp. 147–174.
 - [21] T. Gaitanos, M. D. Toro, S. Typel, V. Baran, C. Fuchs, V. Greco, and H. Wolter, *Nucl. Phys. A* **732**, 24 (2004).
 - [22] E. N. E. van Dalen and H. Mütter, *Phys. Rev. C* **87**, 024317 (2013).

- [23] N. M. Hugenholtz and L. van Hove, *Physica* **24**, 363 (1958).
- [24] G. A. Lalazissis, T. Nikšić, D. Vretenar, and P. Ring, *Phys. Rev. C* **71**, 024312 (2005).
- [25] G. A. Lalazissis, J. König, and P. Ring, *Phys. Rev. C* **55**, 540 (1997).
- [26] B. D. Serot, *Phys. Lett. B* **86**, 146 (1979).
- [27] E. Chabanat, P. Bonche, P. Haensel, J. Meyer, and R. Schaeffer, *Nucl. Phys. A* **627**, 710 (1997).
- [28] B. D. Serot and J. D. Walecka, in *The Relativistic Nuclear Many Body Problem*, Advances in Nuclear Physics, edited by J. W. Negele and E. Vogt (Springer, Berlin, 1986), Vol. 16.
- [29] M. Anastasio, L. Celenza, W. Pong, and C. Shakin, *Phys. Rep.* **100**, 327 (1983).
- [30] C. Horowitz and B. Serot, *Nucl. Phys. A* **464**, 613 (1987).
- [31] B. ter Haar and R. Malfliet, *Phys. Rep.* **149**, 207 (1987).
- [32] R. Brockmann and R. Machleidt, *Phys. Rev. C* **42**, 1965 (1990).
- [33] H. F. Boersma and R. Malfliet, *Phys. Rev. C* **49**, 233 (1994).
- [34] H. Huber, F. Weber, and M. K. Weigel, *Phys. Rev. C* **51**, 1790 (1995).
- [35] W. Kohn and L. Sham, *Phys. Rev.* **140**, A1133 (1965).
- [36] P. Hohenberg and W. Kohn, *Phys. Rev.* **136**, B864 (1964).
- [37] R. Brockmann and H. Toki, *Phys. Rev. Lett.* **68**, 3408 (1992).
- [38] S. Typel and H. Wolter, *Nucl. Phys. A* **656**, 331 (1999).
- [39] A. L. Fetter and J. D. Walecka, *Quantum Theory of Many-Particle Systems* (McGraw-Hill, New York, 1971).
- [40] J. I. Kapusta and C. Gale, *Finite-Temperature Field Theory* (Cambridge University Press, Cambridge, UK, 1989).
- [41] F. Sammarruca, *J. Phys. G: Nucl. Part. Phys.* **37**, 085105 (2010).
- [42] V. A. Karnaukhov, H. Oeschler, A. Budzanowski, S. P. Avdeyev, A. S. Botvina, E. A. Cherepanov, W. Karcz, V. V. Kirakosyan, P. A. Rukoyatkin, I. Skwirczyńska *et al.*, *Phys. At. Nucl.* **71**, 2067 (2008).
- [43] T. Nikšić, D. Vretenar, and P. Ring, *Phys. Rev. C* **66**, 064302 (2002).
- [44] H. Jaqaman, A. Z. Mekjian, and L. Zamick, *Phys. Rev. C* **27**, 2782 (1983).
- [45] G. Peilert, H. Stocker, and W. Greiner, *Rep. Prog. Phys.* **57**, 533 (1994).
- [46] A. Rios, A. Polls, and I. Vidaña, *Phys. Rev. C* **79**, 025802 (2009).
- [47] M. Dželalija, N. Cindro, Z. Basrak, R. Čaplar, S. Hölbling, M. Bini, P. Maurenzig, A. Olmi, G. Pasquali, G. Poggi *et al.*, *Phys. Rev. C* **52**, 346 (1995).
- [48] S. Fiorilla, N. Kaiser, and W. Weise, *Nucl. Phys. A* **880**, 65 (2012).
- [49] B.-A. Li, L.-W. Chen, and C. Ko, *Phys. Rep.* **464**, 113 (2008).
- [50] H.-T. Janka, K. Langanke, A. Marek, G. Martínez-Pinedo, and B. Müller, *Phys. Rep.* **442**, 38 (2007).
- [51] L. F. Roberts, G. Shen, V. Cirigliano, J. A. Pons, S. Reddy, and S. E. Woosley, *Phys. Rev. Lett.* **108**, 061103 (2012).
- [52] R. Wada, K. Hagel, L. Qin, J. Natowitz, Y. Ma, G. Röpke, S. Shlomo, A. Bonasera, S. Typel, Z. Chen *et al.*, *Phys. Rev. C* **85**, 064618 (2012).
- [53] D. T. Khoa and H. S. Than, *Phys. Rev. C* **71**, 044601 (2005).
- [54] R. Furnstahl, *Nucl. Phys. A* **706**, 85 (2002).
- [55] D. V. Shetty, S. J. Yennello, and G. A. Souliotis, *Phys. Rev. C* **76**, 024606 (2007).
- [56] W. Qian, R.-K. Su, and P. Wang, *Phys. Lett. B* **491**, 90 (2000).
- [57] J. M. Lattimer and D. G. Ravenhall, *Astrophys. J.* **223**, 314 (1978).
- [58] C. Ducoin, P. Chomaz, and F. Gulminelli, *Nucl. Phys. A* **771**, 68 (2006).
- [59] G.-H. Zhang and W.-Z. Jiang, *Phys. Lett. B* **720**, 148 (2013).
- [60] H. Huber, F. Weber, and M. K. Weigel, *Phys. Rev. C* **57**, 3484 (1998).
- [61] P. Sahu, T. Jha, K. Panda, and S. Patra, *Nucl. Phys. A* **733**, 169 (2004).